Stem Cell Reports
Article

ISSCR

OPEN ACCESS

Synaptic repair and vision restoration in advanced degenerating eyes by transplantation of retinal progenitor cells

Xiang-Yu He,[1,2,3,4] Cong-Jian Zhao,[1,3] Haiwei Xu,[1,3] Kang Chen,[2] Bai-Shi-Jiao Bian,[1,3] Yu Gong,[1,3] Chuan-Huang Weng,[1,3] Yu-Xiao Zeng,[1,3] Yan Fu,[1,3] Yong Liu,[1,3,*] and Zheng-Qin Yin[1,3,4,*]

[1]Southwest Hospital/Southwest Eye Hospital, Third Military Medical University (Army Medical University), Chongqing 400038, P.R. China
[2]Department of Ophthalmology, the 958th Hospital, Southwest Hospital, Third Military Medical University (Army Medical University), Chongqing 400038, P.R. China
[3]Key Lab of Visual Damage and Regeneration & Restoration of Chongqing, Chongqing, P.R. China
[4]Department of Ophthalmology, General Hospital of Chinese People's Liberation Army, Beijing 100853, P.R. China
*Correspondence: liuyy99@163.com (Y.L.), qinzyin@aliyun.com (Z.-Q.Y.)
https://doi.org/10.1016/j.stemcr.2021.06.002

SUMMARY

Stem cell transplantation shows enormous potential for treatment of incurable retinal degeneration (RD). To determine if and how grafts connect with the neural circuits of the advanced degenerative retina (ADR) and improve vision, we perform calcium imaging of GCaMP5-positive grafts in retinal slices. The organoid-derived C-Kit$^+$/SSEA1$^-$ (C-Kit$^+$) retinal progenitor cells (RPCs) become synaptically organized and build spontaneously active synaptic networks in three major layers of ADR. Light stimulation of the host photoreceptors elicits distinct neuronal responses throughout the graft RPCs. The graft RPCs and their differentiated offspring cells in inner nuclear layer synchronize their activities with the host cells and exhibit presynaptic calcium flux patterns that resemble intact retinal neurons. Once graft-to-host network is established, progressive vision loss is stabilized while control eyes continually lose vision. Therefore, transplantation of organoid-derived C-Kit$^+$ RPCs can form functional synaptic networks within ADR and it holds promising avenue for advanced RD treatment.

INTRODUCTION

Retinitis pigmentosa (RP) is an eye disease characterized by progressive degeneration of rod and cone photoreceptors, leading to progressive loss of vision and eventually blindness. Over 80 different gene mutations have contributed to this disease, marking it one of the most common forms of inherited blindness in the world. In advanced stages of RP when photoreceptors have died, no satisfactory treatments are available due to the absence of cell targets; whereas stem cell transplantation has been suggested to be a promising strategy to replace the retinal cells and restore vision (Scholl et al., 2016; West et al., 2009). We, together with other research groups, had reported that transplanted retinal progenitor cells (RPCs) and photoreceptor precursor cells (PPCs), either isolated from developing retinas or derived from pluripotent stem cells, can replace the damaged cells in RD models (Gonzalez-Cordero et al., 2013; Lamba et al., 2009; MacLaren et al., 2006; Pearson et al., 2012; Zhou et al., 2015). In addition, we conducted a clinical trial to inject fetal RPCs into the subretinal space of RP patients and found that vision was improved to some degree at 3 to 6 months follow-up (Liu et al., 2017). Transplantation of RPCs or PPCs could rescue the visual function of RD; however, two challenging problems need to be addressed. The first problem is how difficult it is to obtain sufficient donor cells. The second one is the mechanism underlying the way in which transplanted cells rescue vision in the degenerative retina.

Regarding donor cells, CD73 is a common marker used to isolate PPCs which have been shown to integrate into the host retina. However, the limited differentiation capacity confines CD73-positive cells to differentiate into the photoreceptor only. Whether CD73 can represent RPCs is still controversial. As we know CD73 is rarely expressed in fetal retina and thus is not able to enrich CD73$^+$ donor cells from immature ESC (embryonic stem cell)-derived retinal organoids (EROs) (Lakowski et al., 2011, 2015). However, on the other hand, extending the culture period to obtain mature human EROs is also challenging. To fill the gap, we reported that C-Kit, a surface marker expressed in both fetal and adult retinas, provides a wide time window for donor cell sorting and the cells sorted by this are ideal for clinical applications. We found that fetal retina- or EROs-derived C-Kit$^+$/SSEA1$^-$ (C-Kit$^+$) cells represent a proportion of RPCs, and these RPCs exhibit good differentiation into retinal neurons without tumorigenic risk post transplantation (Chen et al., 2016; Zhou et al., 2015; Zou et al., 2019). Given the benefit of C-Kit$^+$ grafts in rescuing the vision of early-stage RD models (post-natal day 20 [P20], Royal College of Surgeons [RSC] rats), it is rational to further verify the therapeutic effect of C-Kit$^+$ RPCs in advanced RD.

In terms of therapeutic mechanism, it is apparent that both material transfer and cell integration contribute to protecting the degenerative retina when donor cells are grafted (Decembrini et al., 2017; Ortin-Martinez et al., 2017; Pearson et al., 2016; Sanges et al., 2016; Santos-Ferreira et al., 2016; Singh et al., 2016). Intriguingly, the ratio of integration or material transfer may be determined by the

host microenvironment (Waldron et al., 2018). In the advanced degenerative retina (ADR), the outer nuclear layer (ONL) is significantly thinner, whereas the thickness of the inner nuclear layer (INL) and the ganglion cell layer (GCL) is retained. In addition, the ruptured external limiting membrane allows a large number of donor cells to migrate into the inner neural retina (NR) and form graft-to-host connections with host neurons morphologically. These advantages provide a theoretical framework that can support the substitutional stem cells to integrate into the retina. In our previous study, we observed that the C-Kit$^+$ RPCs were capable of building synapse-like connections with residual retinal neurons in the early degenerative retina (Chen et al., 2016; Zou et al., 2019). These events, although meager, suggest an exciting potential that C-Kit$^+$ RPCs could connect more with host cells in ADR. Nonetheless, the function of these newly formed synapse-like connections has not yet been investigated. Therefore, it is of keen interest to establish a method that allows to delineate the formation of functional contacts rather than morphological connections between graft and host neurons.

To this end, we transplanted mouse EROs (mEROs)-derived C-Kit$^+$ RPCs into an advanced RD model and observed quite a lot of integration events. Graft RPCs and their differentiated offspring cells express a genetically encoded calcium indicator (GECI), allowing whole-graft imaging of activity in multiple cells simultaneously in retinal slices. To address whether the C-Kit$^+$ RPCs can, in fact, connect with the neural circuit of recipient retina, we performed live imaging of implanted cells, which shows differentiation into retinal neurons and exhibition of calcium activities during light stimulation. The grafts responded to host inputs and delivered their own signals through a presynaptic calcium flux similar to that of mature retinal neurons. This indicates that RPC grafts form active synaptic networks within sites of ADR that functionally integrate with the retinal neuron populations and that resemble physiological patterns of neural circuits to the normal retina. Here, we confirm the therapeutic effect of C-Kit$^+$ RPCs and find that vision rescue relies on electrical and synaptic integration in ADR. We are able to provide evidence that the stem cell-based therapy holds enormous promise for replacing neurons lost to advanced neurodegeneration, wherein graft-to-host neural circuits at the injury site are beneficial for preserving vision.

RESULTS

Efficient generation of mEROs from *C-Kit-mCherry; Rosa26*-lsl-*GCaMP5* mESCs

To enable efficient analysis and sorting of C-Kit$^+$ RPCs, we generated a transgenic mouse ESC (mESCs) line with mCherry cDNA knocked in at the locus of the RPC gene *C-Kit*. To facilitate live-cell tracing and Ca^{2+} signaling analysis after cell transplantation, we further knocked calcium indicator GCaMP5 into the Rosa26 locus to generate a *C-Kit-mCherry; Rosa26*-lsl-*GCaMP5* double knockin (DKI) mESC line. Graft cells express GCaMP5, allowing imaging of whole-graft activity simultaneously in multiple donor cells on different retinal layers. A schematic graph showing the gene-targeting strategy to generate the *C-Kit-mCherry; Rosa26*-lsl-*GCaMP5* DKI mESC line is presented in Figure 1A. The DKI mESC line shows similar morphology, characteristics, and neurogenetic ability to the wild type (Figures S1A–S1I and S1T–S1V), except for a slight difference on cell proliferation and differentiation due to genetic modification (Figures S1J–S1M and S1N–S1S). We induced the differentiation based on a previous SFEBq culture protocol to produce donor retinal cells from the 3D optic cup *in vitro* (Eiraku et al., 2011) (Figure S2A). Some RAX$^+$ NR that co-express PAX6, CHX10, and Nestin emerge directly adjacent to the MITF$^+$ retinal pigment epithelium (RPE) and they resemble the optic cup of fetal retina tissue *in vivo* (Figures 1B–1I and S2B–S2E). This indicates that we successfully differentiated DKI mESCs into EROs. Then, we isolated the C-Kit$^+$ RPCs from the mESC-derived NRs and investigated whether these mESC-derived RPCs exhibit similar characteristics to RPCs *in vivo*.

Enrichment of C-Kit$^+$/SSEA1$^-$ RPCs derived from the NRs of mEROs

Spatiotemporal distribution of C-Kit and SSEA1 in NRs of mEROs

Regarding the spatial distribution within the P1 neonatal mouse retina, a strong C-Kit signal was observed in the central region of basal NR, and a weak signal expanded to the apical and peripheral retina (Koso et al., 2007). We observe that the NRs of our mEROs exhibit a large number of C-Kit$^+$ cells. The gray intensity of mCherry in NRs at day 20 is significantly higher than that in other developmental time points (Figure 2A). In NRs at day 20, the intensity of mCherry signal is collectively focused on the basal side of the NR, which recapitulates the INL and GCL of retina *in vivo*. These data indicate that C-Kit is expressed in the NRs of mEROs in a spatiotemporal controlled pattern (Figure 2B).

To determine the optimal time window for cell harvesting, we examined the time course of C-Kit expression in the NRs of mEROs at various developing stages using fluorescence-activated cell sorting (Figure 2C). Unlike previous results that C-Kit expression only peaked in early RPCs during human ERO development (Zou et al., 2019), our result shows that C-Kit expression increases along with mERO development until differentiation day 20, and then decreases over time (Figure 2D). As previously reported, C-Kit expression increased along with mouse development until P1 and then dramatically decreased as the mouse

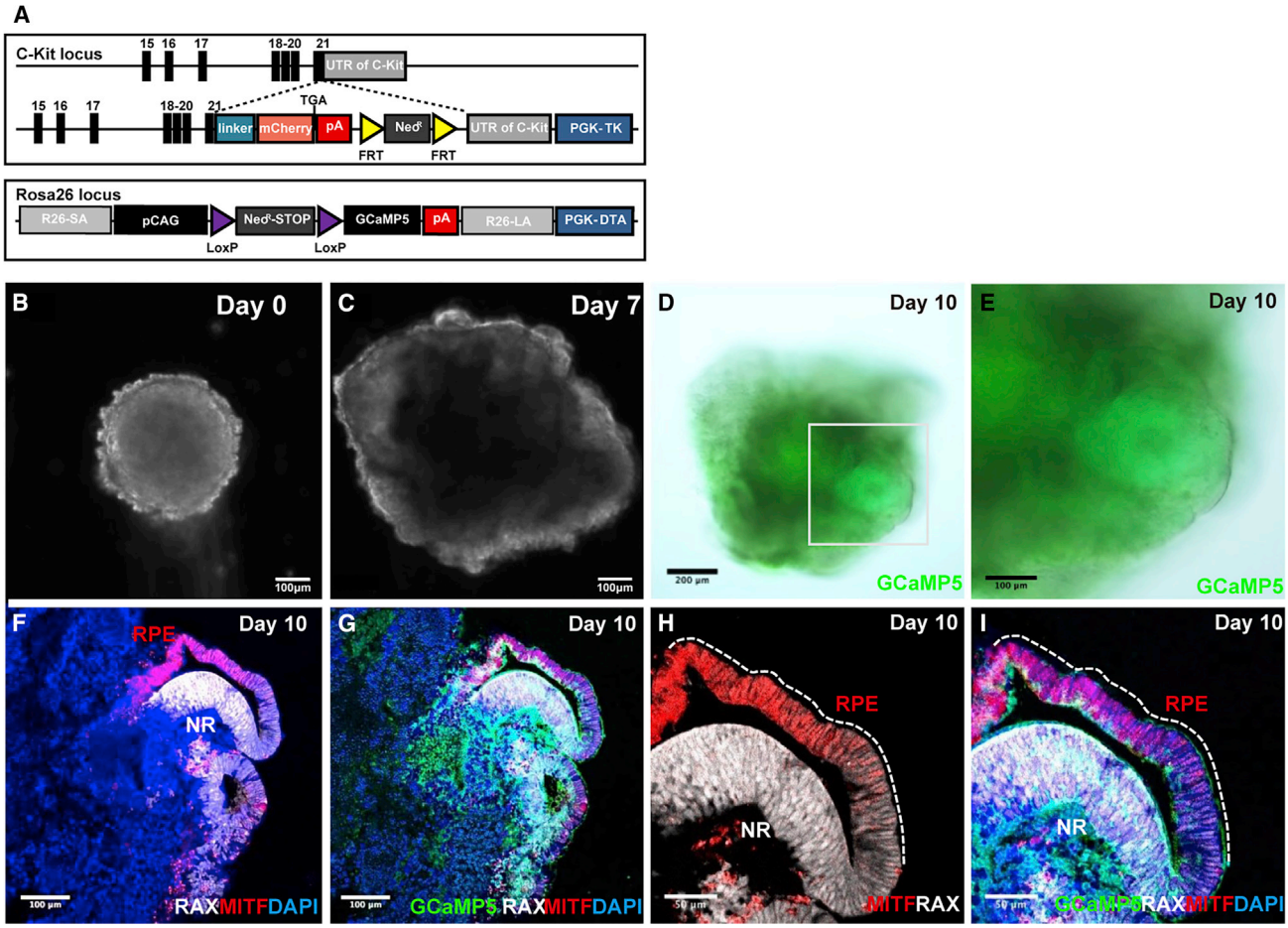

Figure 1. Identification of *C-Kit-mCherry; Rosa26*-lsl-*GCaMP5* mESC-derived retinal organoids

(A) Schematic graph showing the gene-targeting strategy used to generate the *C-Kit-mCherry; Rosa26*-lsl-*GCaMP5* mESC line.

(B–E) Images of mEROs differentiation; re-aggregation of dissociated mESC in a V-bottomed 96-well plate (B), optic-vesicle (C), two-walled optic cup-like retinal anlage (D and E).

(F–I) Both of the inner portion (neural retina) and outer wall (pigment epithelium) expressed calcium indicator GCaMP5 (G and I); within an optic cup-like structure, the neural retina strongly expressed RAX, and the pigmented epithelium strongly expressed MITF (F and H) on day 10. Scale bars, 200 μm (D), 100 μm (B, C, and E–G), and 50 μm (H and I).

retina developed further (Koso et al., 2007). Since the NRs of our mEROs exhibit a C-Kit expressive profile similar to that of the neonatal rodent retina both in time and space orders, these observations prompt further sorting and analysis of C-Kit$^+$ retinal cells in mEROs.

C-Kit$^+$/SSEA1$^-$ cells derived from NRs of mEROs are a subset of RPCs

To prevent tumorigenesis of immature SSEA1$^+$ cells following transplantation, we conducted SSEA1-negative selection for donor cell sorting. We find that the percentage of C-Kit$^+$/SSEA1$^-$ cells in mEROs are 5.68% ± 1.48%, 32.84% ± 3.96%, 61.40% ± 8.71%, and 44.74% ± 9.83% at differentiation days 11, 15, 20, and 27, respectively (Figure 2E) (mean ± standard error of the mean [SEM]). To improve efficiency, we sorted C-Kit$^+$/SSEA1$^-$ cells from day 20 mEROs and cultured them in sphere-formation medium for 10 days. Then, we confirmed that the mEROs-derived C-Kit$^+$/SSEA1$^-$ cells not only possess the capacity of self-renewal but also exhibit the ability to differentiate into major NR neurons (Figures S2 and S3). We proved that these organoid-derived C-Kit$^+$/SSEA1$^-$ cells are a type of RPCs that mimic the robust RPCs derived from fetal rodent retina *in vivo*, and we chose P1 (day 20 mEROs derived) as our source cells for transplantation based on their stable C-Kit expression, evident RPC features, and higher cell viability.

Migration and differentiation of implanted C-Kit$^+$/SSEA1$^-$ RPCs in different retina layers

Previous studies using RCS rats as an RP model have proved that RPCs, including C-Kit$^+$ RPCs, can make

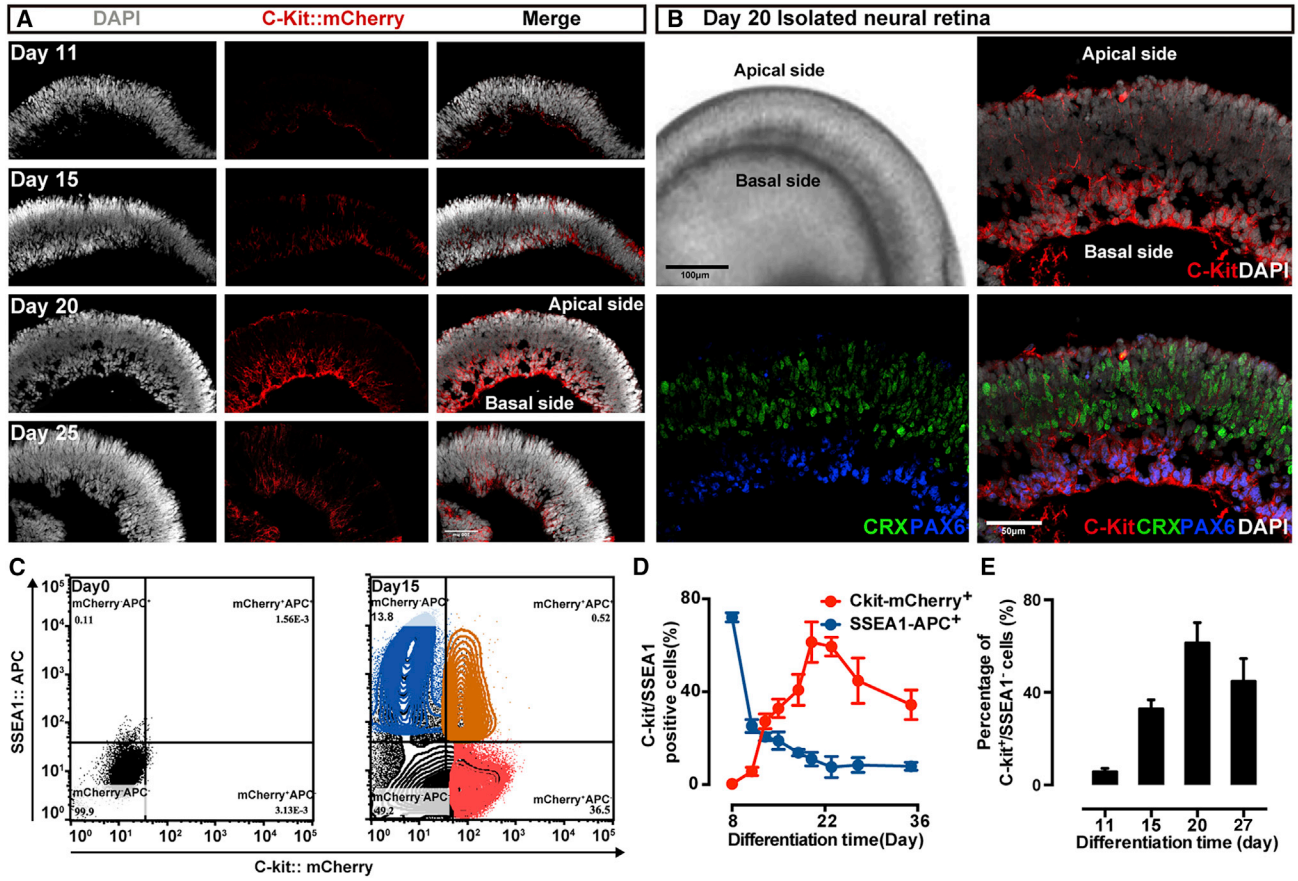

Figure 2. Enrichment of C-Kit^{+}/SSEA1^{-} RPCs derived from mEROs

(A) Distribution of C-Kit-mCherry-positive cells at day 11, 15, 20, and 25 neural retina (NR) of mEROs, The intensity of the signal in the NR was confined to the most central region in a temporospatial manner and peaked at day 20.

(B) At day 20 of mEROs, strong C-Kit expression was observed at the basal side of the NR. Lower panels present an apical-basal pattern of photoreceptors and ganglion cells, immunoreactive for CRX and PAX6, respectively.

(C–E) Flow cytometric analysis of C-Kit expression at various developmental stages of mEROs. Density plot pattern of C-Kit-mCherry versus antibody against SSEA1 at differentiation day 15 (C). Percentage of C-Kit-mCherry-positive cells and SSEA1::APC-positive cells among total NR cells from various developmental stages. Error bars, means ± SEM (C-Kit: day 8, 0.35% ± 0.17%; day 11, 5.68% ± 1.48%; day 13, 27.28% ± 3.19%; day 15, 32.84% ± 3.96%; day 18, 40.83% ± 6.69%; day 20, 61.40% ± 8.71%; day 23, 59.45% ± 4.00%; day 27, 44.74% ± 9.83%; day 35, 34.38% ± 6.35%; SSEA1: day 8, 72.03% ± 1.73%; day 11, 25.28% ± 12.30%; day 13, 20.59% ± 1.64%; day 15, 18.94% ± 3.77%; day 18, 13.75% ± 2.21%; day 20, 11.00% ± 2.93%; day 23, 7.61% ± 4.56%; day 27, 8.42% ± 3.21%; day 35, 7.87% ± 1.54%; n = 3 independent experiments/group; each experiment containing 144 EROs) (D). Percentage of C-Kit^{+}/SSEA1^{-} cells among total NR cells at different developmental stages (day 11, 5.68% ± 1.48%; day 15, 32.84% ± 3.96%; day 20, 61.40% ± 8.71%; day 27, 44.74% ± 9.83%; Error bars, means ± SEM; n = 3 independent experiments/group; each experiment containing 144 EROs) (E). Percentages were calculated by using FlowJo v.X.0.7 software. Scale bars, 100 μm (J).

mature photoreceptors and alleviate functional defects (Bian et al., 2020; Zou et al., 2019; Zhou et al., 2015; Luo et al., 2014). Notwithstanding the fact that material transfer and cell fusion contributed to a proportion of rescue following RPCs transplantation (Sanges et al., 2016; Santos-Ferreira et al., 2016; Singh et al., 2016), a substantial number of RPCs were capable of integrating into the host retina when the retinal structure was disrupted in advanced degeneration (Waldron et al., 2018). To observe more integration events, we performed transplantation to late-stage degenerative retina in day 63 RCS rats (P63) (Figure 3A). The retinal degeneration stages were determined by flash electroretinogram, which was barely detectable in P63 or older RCS rats. If the reporter-labeled cells transferred material or fused to the recipient cells, we could track them directly by fluorescence. In addition, the transplanted cells were male and the recipient rats were female, and we could trace them by fluorescence *in situ*

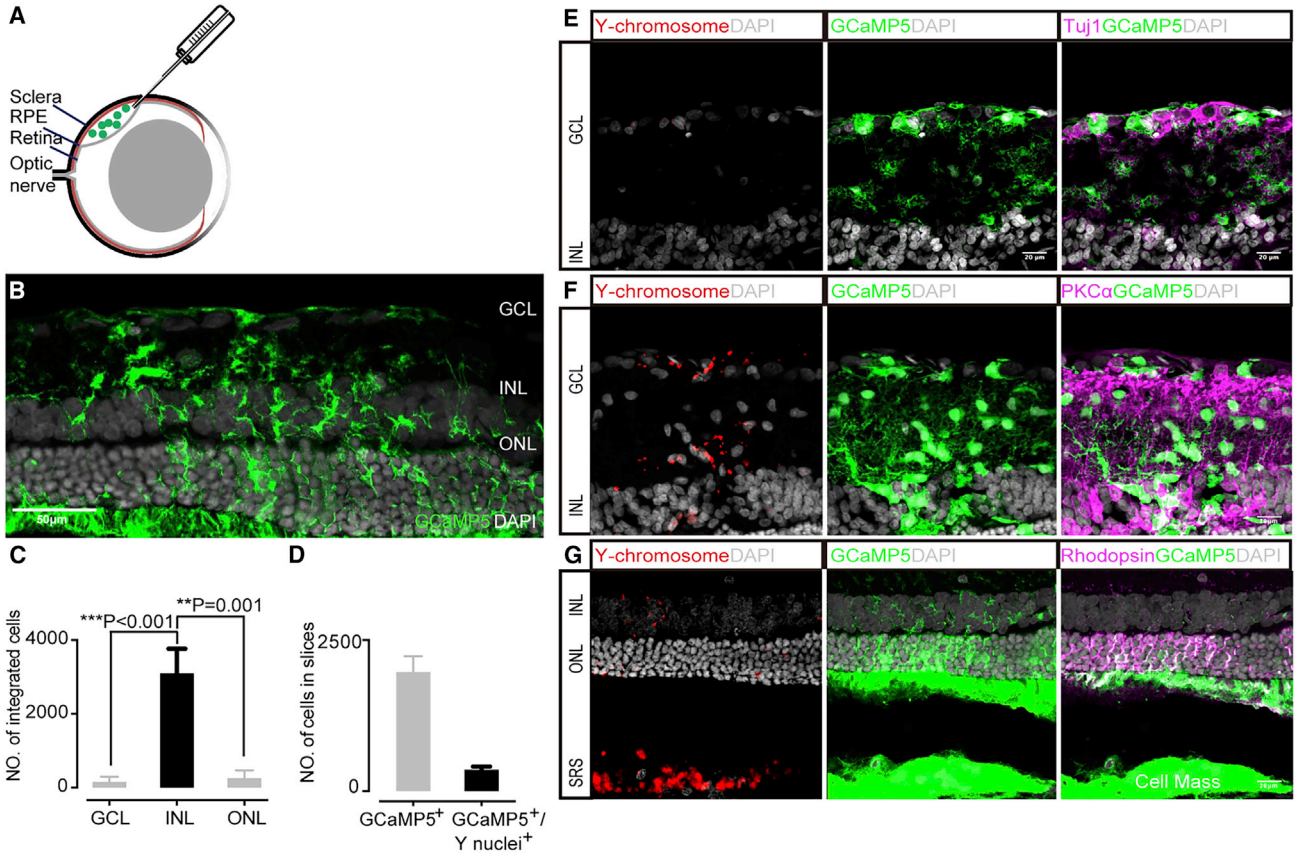

Figure 3. Migration and differentiation of implanted C-Kit$^+$ RPCs in RCS rats

(A) Schematic graph showing the subretinal transplantation of C-Kit$^+$ RPCs.

(B) A representative example of integrated C-Kit$^+$ RPCs (GCaMP5$^+$, green).

(C) Histogram showing the distribution of Y$^+$ nuclei at ONL, INL, and GCL. 158 ± 53 cells located at the GCL, 3,098 ± 665 cells located at the INL, and 262 ± 78 cells located at the ONL. Error bars, means ± SEM (n = 5 independent experiments and serial cryosections counted per experiment; the average number of cells that integrated in each eye was determined by counting all integrated cells in each serial section). *p <0.05, **p < 0.01, ***p < 0.001, by t test.

(D) Statistical analysis of the number of the GCaMP5$^+$ cells (1972 ± 261) and GCaMP5$^+$/Y$^+$ cells (354 ± 54); 21% ± 4% GCaMP5$^+$/Y$^+$ cells in all retina layers. Error bars, means ± SEM (n = 10 eyes; containing 19,719 GCaMP5$^+$ cells).

(E–G) Representative images of the migrated transplanted cells: 158 ± 53 cells located at the GCL (E), 3,098 ± 665 cells located at the INL (F), and 262 ± 78 cells located at the ONL (G). Co-expression of retinal-specific markers Tuj1 (ganglion cells), PKCα (bipolar cells), and Rhodopsin (photoreceptors) in implanted cells were obtained. Scale bars, 50 μm (B) and 20 μm (E–G).

hybridization (FISH) for Y chromosome (Y$^+$) if fused post transplantation.

To characterize the pattern of cell differentiation and integration, the recipient retinas (n = 6) were examined by immunofluorescence and FISH (Figures 3A–3F). First, by using immunofluorescence and confocal imaging (Figure S4A), we found that a majority of Y$^+$ nuclei remain in the subretinal space without migration and up to 7537 Y$^+$ nuclei are distributed across three different nuclear layers of the recipient retina (3,518 ± 796 cells) (Figure 3C) (mean ± SEM). The majority of GCaMP5-labeled cells are located within the ONL of host retina, among them very limited cells are Y$^+$ nuclei (Figure 3G). Among the GCaMP5$^+$ cells (1972 ± 261), 21% ± 4% of the GCaMP$^+$ cells colocalize with Y$^+$ nuclei (354 ± 54) (Figure 3D) (mean ± SEM, n = 10 eyes; containing 19,719 GCaMP5$^+$ cells). These results are kind of expected due to the fact that C-Kit$^+$ cells can differentiate into PPCs and possess material transfer with resident cells (Pearson et al., 2016; Zou et al., 2019). However, an increased number of Y$^+$ nuclei are observed within the INL and GCL of host retinas (Figures 3E and 3F). This result indicates that most reporter-labeled cells within ONL are derived from material transfer not migration of donor cells, while most GCaMP5$^+$ cells found in the INL are originated from donor cell implantation. A previous study has examined the spatial localization of C-Kit$^+$ RPCs in developing retina and found a strong

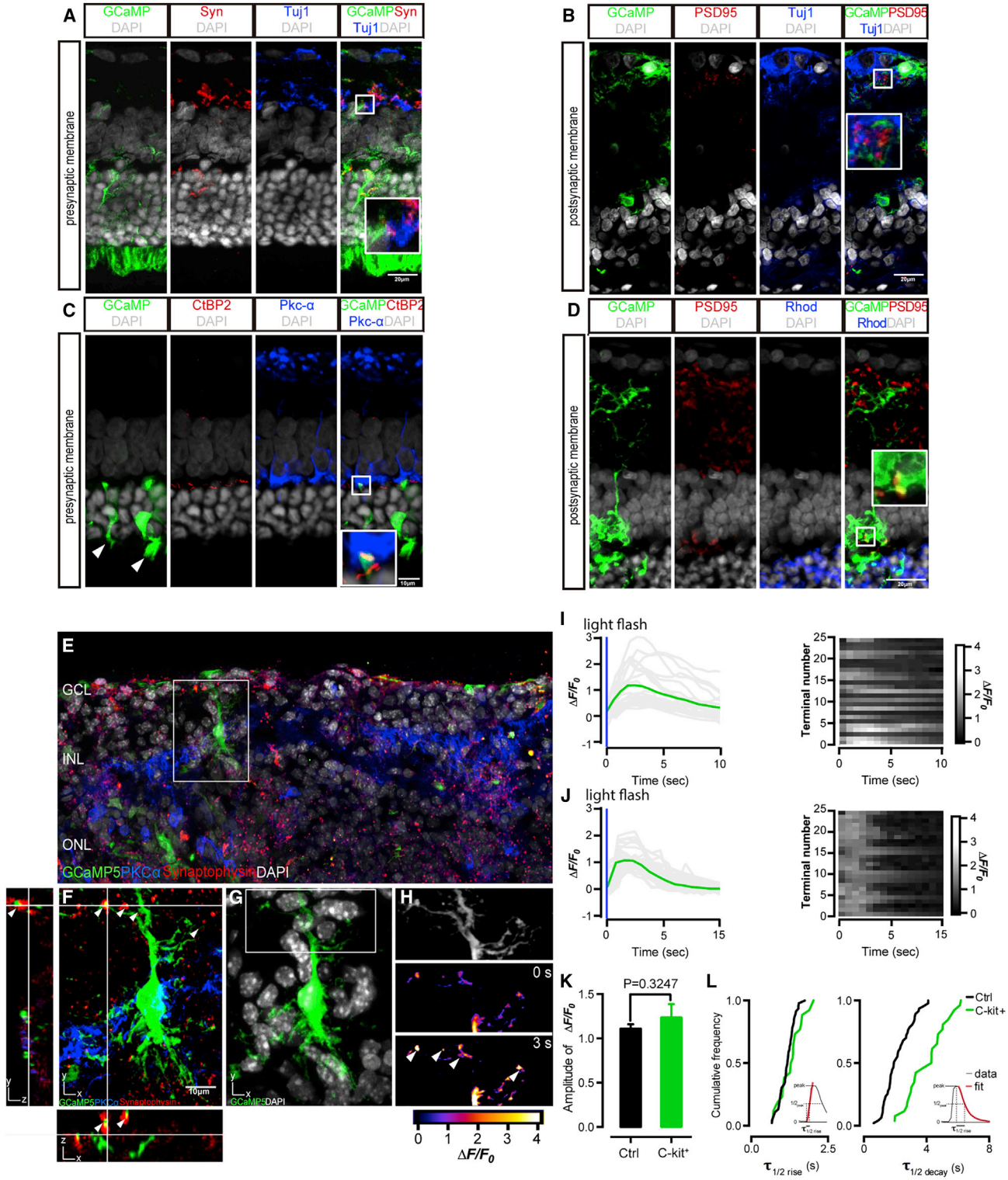

Figure 4. Functional graft-to-host synapses formed by C-Kit$^+$ RPCs in RCS rats

(A–D) Integrated C-Kit$^+$ RPCs formed graft-to-host synapses and expressed presynaptic marker synaptophysin (A), presynaptic marker CtBP2 (C), and postsynaptic marker PSD95 (B and D) (all red), counterstained with RGC marker Tuj1, bipolar marker PKCα, and photoreceptor marker Rhodopsin. White arrows mark outer segments (C).

(legend continued on next page)

C-Kit expression in the INL and GCL within the central region of the retina in the neonatal mouse retina (Koso et al., 2007). Intriguingly, most of the graft C-Kit$^+$ RPC here are distributed in the INL, where C-Kit is dominantly expressed in neonatal mouse retina. This suggests that there might be a stem cell niche in the INL layer to support the survival of C-Kit$^+$ RPCs. We found that the integration efficiency is determined not only by the general host environment but also by the local retinal laminar environment.

Due to technical limitations, most detailed information of the GCaMP signals, such as neuron cell processes are lost when overlapping with Y-probe staining (Figure S4B). To determine if calcium signals arise from implanted cells rather than material transfer, we counterstained mouse nuclei with calcium imaging. The antibody (Abcam, ab134014) used in the assay was NeuN (C-terminal), which is only reactive to mouse species. Although the anti-NeuN antibody cannot label all retinal neurons (Mullen et al., 1992), the NeuN-labeled nuclei exclusively belong to donor cells. Intriguingly, all cells labeled with NeuN (NeuN$^+$) show GCaMP fluorescence activity, while a proportion of cells that are not labeled with NeuN (NeuN$^-$) show GCaMP fluorescence quiescence (Figures S5A and S5B). Furthermore, we performed quantification of Y$^+$ nuclei in the same sections, and data show that NeuN$^-$ cells with GCaMP fluorescence active are immature in morphology and positive for Y-probe staining (n = 116/116, N = 4), whereas NeuN$^-$ cells without GCaMP fluorescence are negative for Y-probe staining (n = 372/372, N = 4) (Figures S5C and S5D). Taken together, cells that located in the INL and were GCaMP fluorescence active and morphologically immature are inferred to be donor cells. To eliminate the interference of material transfer on cell integration, the GCaMP$^+$ cells mentioned thereafter are all fluorescence-active cells.

Formation of functional synapses by the donor C-Kit$^+$/SSEA1$^-$ RPCs

In wild-type rodent retina, synaptophysin (Syn) is located at the presynaptic membranes and PSD95 is located at the postsynaptic membranes of retinal neurons. At 28 days post operation (PO), the synaptic junctions between C-Kit$^+$ cell-derived neurons and host retina express Syn, which colocalized with GCaMP5 fluorescence (Figure 4A). This result implies that Syn is expressed on the presynaptic terminals of C-Kit$^+$ cell-derived neurons. Meanwhile, PSD95 is colocalized with dendritic terminals of donor cell-derived neurons, as labeled by Tuj1 and Rhodopsin (Figures 4B and 4D), which implies that PSD95 is expressed on the postsynaptic dendrites. Then, we used CtBP2, a presynaptic protein typically expressed at photoreceptor terminals, to verify the ribbon-type synapses (Figure 4C). In the merged image, CtBP2 colocalize with terminals of implanted cell and are adjacent to the dendritic process of bipolar cell in OPL (magenta fluorescence, Pkc-α^+). This indicates that C-Kit$^+$ RPC-derived rods are integrating with outer segment formation (Figure 4C, arrow) and form typical ribbon-type synapses with correct spatial alignment in the OPL. Taken together, these data indicate that the implanted C-Kit$^+$ cells are morphologically integrated with the host cells and formed synapses in the retinas of RCS rats.

The calcium influx that was measured in the presynaptic compartment reflects the synaptic transmission driven by release of synaptic vesicles (Katz and Shatz, 1996). To confirm the functionality of the newly formed synapses, we conducted two-photon imaging by localizing GECI (GCaMP5) to the presynaptic terminal of integrated donor cell and detected the calcium influx, which was triggered by neurotransmitter release. In response to a brief light flash (spatially uniform flashes from a linearized, calibrated light-emitting diode [LED]; full-field LED, 458 nm, 125 ms duration, 100 $\mu W/cm^2$), we monitored the fluorescence changes in presynaptic terminals of integrated GCaMP5$^+$ cell in INL of live retina slices (28 days PO) (Figure 4E). Meanwhile, we monitored the changes of fluorescence in INL terminals, which were labeled with the calcium indicator Fluo-4 AM, as a control group in the congenic rat (RCS-*rdy*$^+$ rats) retina. After the conduction of photoreceptors, light flash-evoked fluorescence is detected in presynaptic

(E and F) Immunofluorescence of the integrated cells showing the co-expression of GCaMP5 and synaptophysin, indicating the generation of synaptic connections. (F) Terminals responding to light (white arrows) confirm the activities of presynaptic calcium transient using two-photon live imaging.

(G) Fluorescence image of integrated cell expressing GCaMP5.

(H) Region of interest corresponding to single synaptic bouton in the confocal image.

(I and J) The GCaMP5 fluorescence responses (left panels, gray traces and their average in green trace) and the raster plots showing fluorescence responses (right panels) from 25 terminals of integrated cells (I) and control cells (J), respectively, elicited by a brief light flash shown as a blue bar. Imaging frequency, 1 Hz; 256 × 256 pixels.

(K) Filter time-to-peak across the recorded integrated cells (green bar) and control cells (black bar) (each group n = 25, t test, p = 0.34, not significant). Error bars indicate SEM.

(L) Cumulative frequency histograms of fluorescence response kinetics for GCaMP5-labeled integrated cells (green) and control cells (black). Left, rise kinetics; right, decay kinetics. Insets, fits for $t_{1/2}$ (rise) and $t_{1/2}$ (decay). Scale bars, 20 μm (A, B, and D) and 10 μm (C and F).

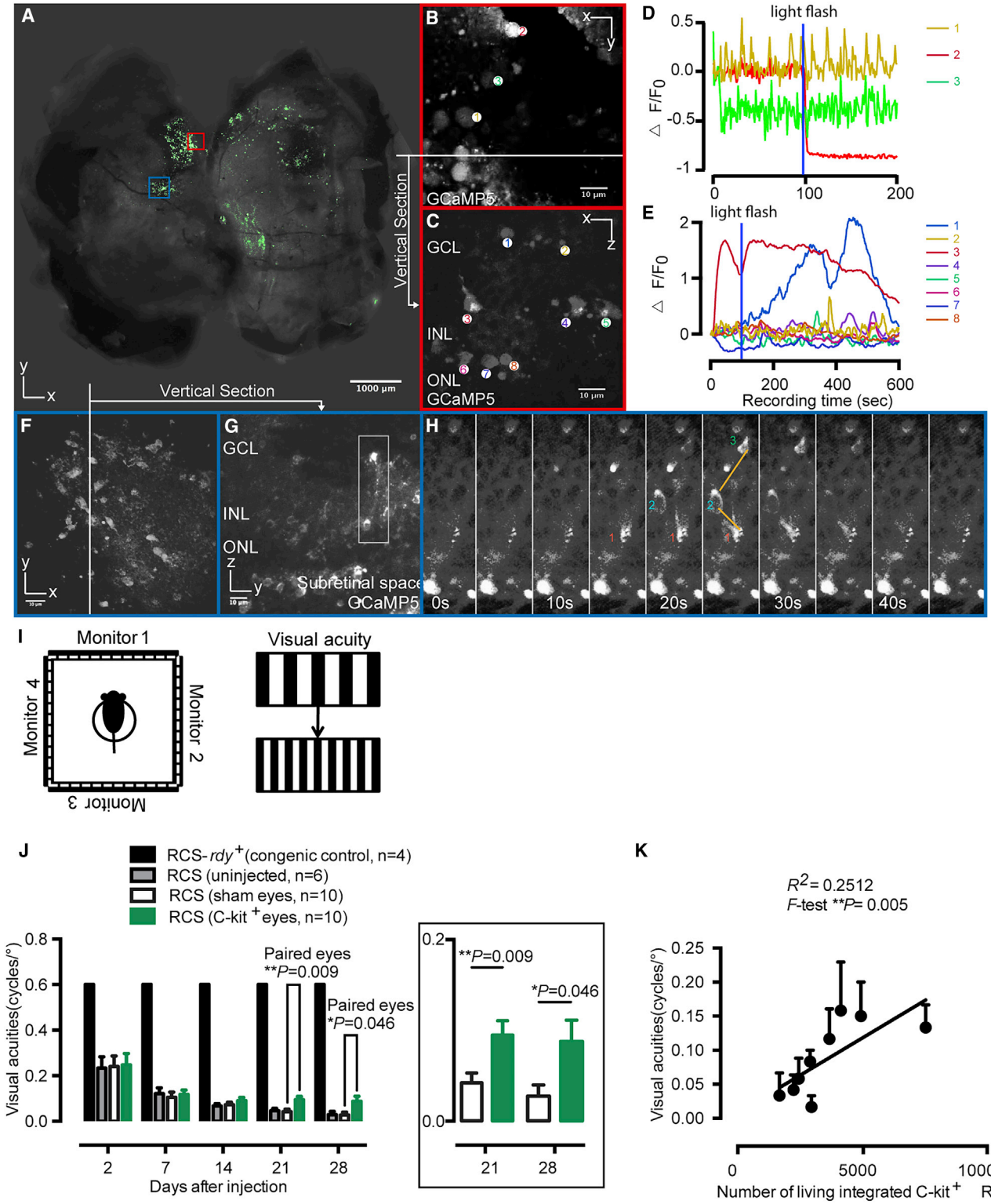

Figure 5. Rescue of optokinetic head-tracking behavior in C-Kit+ RPC-treated RCS rats

(A) The flat mount of recipient retina shows the distribution of the injected cells across the whole retina.

(B–H) Two-photon imaging and fluorescence response of GCaMP5-labeled implanted cells in whole-mount preparations and a live sections of recipient retina. (B and F) Representative images of the implanted cells. The traces show the fluorescence response measured from the

(legend continued on next page)

terminals of both experimental groups (Figures 4H and 4I) and the control group (Figure 4J). The peak GCaMP5 signal $\triangle F/F_0$ (see the supplemental information) is 0.078 ± 0.003 in integrated donor cells, and 0.104 ± 0.003 in INL terminals of control retina neurons. Although varying intensities of signals have been detected between different terminals, integrated donor cells exhibit a presynaptic calcium transient similar to that of mature retinal neuron when measured in response to light—both showing similar $\triangle F/F_0$ response amplitude, response time-to-peak, and response duration (Figure 4K). The temporal kinetics of fluorescence response in integrated donor cells is slightly slower than those in mature retinal neurons (half-rise: 200 ± 8 ms for integrated cells, n = 25; 170 ± 30 ms for controls, n = 25; not significant, p = 0.39, t test; half-decay: 710 ± 8 ms for donor cell, n = 25; 630 ± 10 ms for control, n = 25; significant, p < 0.0001, t test) (Figure 4L).

Combined with confocal imaging (Figures S4A and S4B), we determined that the location of calcium responses is exactly overlapped with the immunofluorescence-labeled synaptic terminals (colocalization of GCaMP5 and synaptophysin) (Figures 4F–4H). Although the donor cell cannot perceive light stimulation itself, it can accept the neural impulse transmitted by the surrounding host cells and convey a corresponding calcium response by releasing synaptic vesicles. Based on this evidence, we show that the donor C-Kit$^+$ RPCs have reconstructed the graft-to-host connections and remodeled functional synapses in the ADR.

Implanted C-Kit$^+$ RPCs preserved visual acuity in advanced retina degenerative RCS rats

In whole-mount retina, the GCaMP5-labeled donor cells are generally distributed around the injection site, whereas some other clusters of cells are sparsely distributed across 30% of the retina (Figure 5A). To characterize the expression pattern and fluorescence response of GCaMP5 in transplanted RPCs (Figures 5C–5H), we conducted two-photon imaging in whole-mount retina (Figures 5A, 5B, and 5F) and live retina slices (Figures 5C, 5G, and 5H). The viability and functions of GCaMP5$^+$ cells within the recipient retina were investigated. We found that all the somas and neurites of injected cells were labeled with GCaMP5 fluorescence at a micrometer resolution in two-photon microscopy (Figures 5C and 5F–5H). The GCaMP5 fluorescence shows a variety of intensities of Ca^{2+} activities in response to the brief light flash (Figure 5D) or scan laser light (Figure 5E) (slow, fast, and even with opposing intensities), which reflects a diversity of donor cell-derived retinal neurons, including sluggish and brisk, ON and OFF. The intensity amplitudes are distributed from −89% to 209% ($\triangle F/F$) within the cell soma (Figures 5C and 5E). To test whether the implanted cells work like normal retina neurons, we compared Ca^{2+} activities of implanted cells with those of normal congenic rats. The control rats were labeled with calcium indicator Fluo-4 AM, which is responsive to the brief light flash, and delivered 2 s after two-photon scan onset. Similar light-evoked fluorescence changes are observed in the donor cells at the three retina layers (GCL, INL, and ONL) and the control intact retina (Figures S5E–S5G). Moreover, GCaMP5-labeled donor cells synchronize their activities with neighboring cells (Figure 5H). This result indicates that calcium signals can be transmitted between GCaMP5$^+$ cells through electrical synaptic connections, such as gap junctions (Akrouh and Kerschensteiner, 2013).

To address whether C-Kit$^+$ RPC transplantation confers vision improvements, we further examined the visual function through a highly sensitive method—the optokinetic head-tracking response (Figure 5I). In this experiment, moving gratings are used to elicit the visually dependent optomotor response of RCS rat. The visual acuity test includes eight spatial frequencies. By increasing the spatial frequency until the animal no longer tracks, the visual acuity in each eye can be estimated (Prusky et al., 2004). Each rat received C-Kit$^+$ RPC transplantation in one eye and sham injection in the contralateral eye. An additional two cohorts were eyes of normal congenic rats and eyes of RCS rats that received no injection. As expected, poor but detectable head-tracking behavior was observed in the RCS rats before transplantation and normal head tracking was detected in normal congenic rats (Figure 5J). After transplantation, the visual acuities are significantly better compared with the vehicle or untreated control (0.095 ± 0.014 versus 0.043 ± 0.011 cycles and 0.046 ± 0.010 per degree at day 21 post-injection, 0.085 ± 0.018 versus 0.028 ± 0.012 and 0.029 ± 0.010 at day 28 post-injection) (mean ± SEM) (Figure 5J). The number of integrated cells with fluorescence changes was determined and there was a significantly

whole-mount retina (B and F) and retinal slice (C and G). (H) Implanted cells synchronized their activities with the adjacent-layer cells by transmitting calcium signals through electrical synaptic connections (calcium flux transmitted from cell 1 through cell 2 to cell 3). (D and E) A brief blue light flash (458 nm, 125 ms duration, 100 $\mu W/cm^2$) evoked fluorescence responses.

(I) Schematic of the optokinetic head-tracking response tests performed on RCS rats.

(J) Visual acuity threshold measurements for C-Kit$^+$ RPC-treated (green bars) or sham-treated (white bars) RCS rat eyes, and the averages of eyes for untreated RCS rats (gray bars) or normal congenic (black bars) controls. Paired t test.

(K) Correlation plot of visual acuity against the number of integrated C-Kit$^+$ RPC, with $R^2 = 0.2512$ (p = 0.005). Error bars, means ± SEM; n, number of animals. Scale bars, 1,000 μm (A) and 10 μm (B, C, and F–H).

positive correlation with visual acuity (F test, **p = 0.005; Figure 5K). The results presented here demonstrate that the transplanted mEROs-derived C-Kit$^+$ RPCs restore vision in ADR.

DISCUSSION

Recent studies have showed that cell transplantation can restore visual function in animal models of RD (Mandai et al., 2017; Pearson et al., 2012). In this study, we confirm that the engrafted mEROs-derived C-Kit$^+$ RPCs can reverse advanced retinal degeneration and preserve vision. The engrafted RPCs are genomically edited to express a GECI, namely GCaMP5, to facilitate whole-graft tracing. We find that the C-Kit$^+$ RPCs are able to migrate into the inner retina and differentiate into major neurons in three retinal layers, including photoreceptors, interneurons, and ganglion cells. These transformations result in a considerable number of cells that form morphological synaptic connections with residual retinal neurons in an advanced RD retina. To gain insight into the nature of synaptic connectivity and functionality between regenerating host-graft synapses and neurons, we performed live imaging of calcium activity by light stimulation in RPC injection sites. We found that the light-stimulated photoreceptors elicited robust and widespread calcium responses to photosensitive- and non-photosensitive graft neurons. Likewise, graft neurons in INL generate a correlated electric activity, known as transient presynaptic calcium flux, back to host neurons similar to that of mature retinal neurons. The neural interaction between graft-to-host cells is similar to that neural activation of circuits in intact retina. When the grafted neurons perceive light stimuli from the host, they respond by delivering their own signals to form synapses connecting to the host. Once network wires cohesively, a neural circuit is established, and the grafted cells are formally and functionally integrated with the host retina. While the long-term effect by which graft C-Kit$^+$ RPCs reform retinal circuits remains to be elucidated, our findings suggest that the stem cell replacement could be beneficial for a wide range of patients with RP, and potentially for other patients with function impairment that affect vision or other areas of the central nervous system.

Although RPCs and PPCs are a promising source of donor cells for transplantation, debates regarding the cellular mechanism for functional rescue remain. While migration and integration of donor cells contribute to the functional rescue, material transfer and cell fusion also take place when the donor cells are grafted into the host retina (Decembrini et al., 2017; Ortin-Martinez et al., 2017; Sanges et al., 2016; Singh et al., 2016). The fact is that the integration accounts for far less of the reporter-labeled cells (Pearson et al., 2016). We chose 63-day-old RCS rats as advanced RD models, because they have no ERG response. At that point in time, the degeneration has advanced to extensive thinning of ONL and disrupted structure of the outer limiting membrane (OLM). The OLM is a barrier before degeneration, and it becomes porous and more permissive for donor cells to migrate into the inner retina. Moreover, studies found that immature RPCs engaged less effectively in material transfer (Pearson et al., 2016; Santos-Ferreira et al., 2016). For this reason, we transplanted C-Kit$^+$ RPCs instead of post-mitotic retinal neurons into ADR, to engage a measurable ratio of integration. As a result, our ratio of actual integration events is ~1:5, while it was only ~6:100 in a previous study (Zou et al., 2019). Although we cannot rule out the effect of material exchange after transplantation, we attribute this outstanding therapeutic effect to a cell-replacement mechanism, which is the functional synaptic reconstruction between C-Kit$^+$ RPCs and the residual retinal neurons, especially when the recipient retina shows advanced degeneration.

Previously, the presence of graft-host connectivity was usually identified morphologically in the retina (Chen et al., 2016; Gonzalez-Cordero et al., 2013; Pearson et al., 2012; Zou et al., 2019). In the central nervous system (CNS), previous studies examined graft-host connectivity and relay formation by host stimulation and recording on either side of a graft (Koffler et al., 2019). This method did not define the exact cell population being recorded due to the diffused electrical current throughout the tissue. The patch clamp is an accurate method to examine the function of graft-host synapses, but it is not applicable to test a massive amount of cells. Yet calcium imaging can detect graft neurons responding to neural input (Ceto et al., 2020). GCaMP5, a GECI, is a powerful tool for testing neurofunction, especially in cortical neurons. In the retina, GCaMP labeling enables functional imaging of calcium dynamics in dendrites, somas, and axonal arbors, and these can be compared between multiple retinal neurons of either the same type or different types (Borghuis et al., 2011). In our study, GCaMP5 fluorescence of axons or dendrites in the plexiform layer could be traced back to the soma of a typical retinal neuron (Figures 5C, 5G, and 5H), indicating that GCaMP5 fluorescence can record excitable neuron populations derived from donor RPCs. Using a two-photon microscope in live retina slices, we detected the migration of the GCaMP5$^+$ RPCs into all three layers of the recipient retina, where they form synaptic structures that colocalize within the functional zone, similar to the retinal synapses. Moreover, function improvement was also confirmed by a significant preservation of visual acuity in an optokinetic head-tracking test. Altogether, our EROs-derived C-Kit$^+$ RPCs reconstruct synapses with the residual retinal neurons and enhance the function of recipient

neural circuits. Consequently, the signal transmission of the dystrophic retina is increased and vision is preserved in advanced RCS rats.

In conclusion, we have developed a strategy to evaluate cell integration functionally by using calcium imaging rather than detecting gene/protein expression markers. We present evidence to support the use of EROs-derived RPCs in advanced RD, and have shown exceptionally robust synaptic repair and restoration of vision. Our study, for the first time to our knowledge, has shown that mEROs-derived C-Kit$^+$ RPCs can form functional synapses with the host cells and connect with the neural circuit of the ADR. Our findings support that stem cell transplantation might become a feasible and promising avenue for CNS lesions beyond advanced retinal degeneration.

Limitations of study

After transplantation, we noticed that a certain number of donor GCaMP5$^+$ cells migrated into the inner plexiform layer (IPL). Immunofluorescence showed that these cells are co-stained with Nestin, Pkc-α, and Tuj1. It is clear that the donor cells in the IPL layer are a mixed population of a variety of ectopic cells, including precursor cells, ganglion cells, bipolar cells, etc. (Figures S4C–S4E). The abnormal discharge of these cells may disrupt the synaptic circuits in the inner NR. How to induce the correct distribution of these migrating donor cells will be a focus of future research.

The microenvironment of the advanced retinal degeneration model is obviously worse than moderate degeneration, which results in less survival of C-Kit$^+$ RPCs and a short-lived transplantation effect. We did not follow up on a long period of time post RPC transplantation. The mutation in the proto-oncogene *mer tyrosine kinase* of the RCS rat can lead to deficient phagocytosis in the RPE cells. In this way, it contributes to photoreceptor out segment accumulation in the subretinal space, which ultimately results in retinal degeneration (Mullen and LaVail, 1976; D'Cruz et al., 2000). For this reason, reestablishing the defect of RPE function is very important for alleviating advanced RD. To achieve a long-term effect, a combined transplantation of RPCs and other trophic support cells, such as RPE cells, is warranted. Whether the transplantation can preserve the electrophysiological function, such as ERG waves, is expected to be disclosed by future studies. Such investigations will require more integrated cells and their mature differentiated offspring cells.

EXPERIMENTAL PROCEDURES

Animals

RCS rats and congenic control RCS-rdy+ rats were provided by the Experimental Animal Center of Third Military Medical University (Army Medical University). All animal were maintained by the Institutional Animal Care and Use Committee of the Third Military Medical University (Army Medical University). All animal work has been approved by the Institutional Review Board of the Third Military Medical University (Army Medical University). All treatments were conducted in accordance with NIH guidelines for the care of laboratory animals and the ARVO Statement for the Use of Animals in Ophthalmic and Vision Research. The animals were housed under a standard 12-hr light-dark cycle. All visual function tests were conducted within the light phase. The adult rats were 21 days old at the time of cell injection. All recipients were restricted to drinking water containing 210 mg/l cyclosporine A starting from the day before transplantation to the day of euthanization.

Gene-targeting strategy and plasmid construction

C-Kit-mCherry and Rosa26-pCAG-GCaMP KI vector construction: the mCherry sequence was knocked into the upstream of the C-Kit stop codon in exon 21 (in frame). Linker between C-Kit and mCherry: a flexible linker (GGGGS) between C-Kit and mCherry was used to improve the folding and stability of the C-Kit-mCherry fusion protein. Properly targeted ESCs were identified by PCR and Southern blot. Then, a GCaMP expression cassette driven by the CAG promoter was knocked in the intron of the Rosa26 locus to generate the Rosa26-pCAG-GCaMP vector. Properly targeted ESCs were identified by PCR and Southern blot. The neomycin cassette was removed by electroporation of the Cre plasmid. The C-Kit-mCherry and Rosa26-pCAG-GCaMP ESCs were generated with the assistance of Nanjing Biomedical Research Institute of Nanjing University (Figure 1A).

Preparation of low-gelling temperature agar-embedded live retina slices

Animals were dark-adapted overnight before anaesthetization with pentobarbital sodium. Then, animals were sacrificed by cervical dislocation. The eyeballs were quickly enucleated and placed in slicing solution (comprising: 119 in mM NaCl, 2.5 in mM KCl, 0.25 in mM $CaCl_2$, 3.2 in mM $MgCl_2$, 12 in mM D-glucose, 0.2 in mM L-ascorbic acid, and 12 in mM HEPES [pH adjusted to 7.4 with NaOH, osmolarity adjusted to 260 mOsm using water and 10× stock solution]), bubbled with 95% O_2/5% CO_2, before cervical dislocation. Each eye was subsequently hemisected, and the anterior half and the lens were discarded. Next, the NR was carefully removed from retinal pigmented epithelium and radially cut into three to four pieces. The retinal pieces were embedded with 3% low-gelling temperature agarose (Sigma), and the agarose was solidified with an ice-cold slicing solution. A solid agarose block containing a rectangular piece of the retina was cut into 200–250-μm-thick slices using a vibratome slicer in ice-cold slicing solution. The agarose-embedded retinal slice was then transferred to recording solution (comprising: 100 in mM NaCl, 2.5 in mM KCl, 2.5 in mM $CaCl_2$, 1 in mM $MgCl_2$, 12 in mM D-glucose, 0.2 in mM L-ascorbic acid, 25 in mM $NaHCO_3$ [pH adjusted to 7.4 with NaOH after bubbling the solution with 95% O_2/5% CO_2 for 10 min, osmolarity adjusted to 260 mOsm using water and 10× stock solution]) to perform optical recordings.

Optical calcium-imaging recordings using two-photon microscopy

Calcium imaging was performed using a moveable objective microscope (Sutter) equipped with a Chameleon titanium-sapphire laser tuned to 915 nm (Coherent), employing an Olympus LUMPlanFI 40× water immersion objective (NA 0.8). Emitted fluorescence was captured by the objective and filtered using an HQ 535/50GFP emission filter (Chroma Technology) before detection using Pho Image v.3.0 software3, run on a PC. Images were acquired at a resolution of 256 × 256 pixels. Image sequences were acquired at 1 ms per line using 256 × 256 or 128 × 128 pixels per frame and analyzed with Igor Pro v.6.10 or ImageJ v.1.46 (NIH). The regions of interest were defined by the standard deviations of image sequences. Scanning and image acquisition were controlled using scan normalized fluorescence responses calculated as follows:

$$\Delta F \Big/ F = \frac{F - F_0}{F_0},$$

where F is the instantaneous GCaMP5 fluorescence, and F_0 is the baseline GCaMP5 fluorescence.

Statistical analysis

The data are presented as the means ± SEM. Student's t test was used for paired and unpaired comparisons. All statistical analyses were performed using the SPSS software package (version 11.0; SPSS, Chicago, IL, USA), and $p < 0.05$ was considered a significant difference.

SUPPLEMENTAL INFORMATION

Supplemental information can be found online at https://doi.org/10.1016/j.stemcr.2021.06.002.

AUTHOR CONTRIBUTIONS

X.Y.-H. designed the study, collected and assembled the data, analyzed and interpreted the data, and wrote the manuscript. X.Y.-H., C.-J.Z., K.C., C.-H.W., and Y.-X.Z. performed the experiments. C.-J.Z. and H.X., wrote the manuscript. B.-S.-J.B., Y.G., and Y.F. collected and assembled the data. Y.L. conceived and designed the study, wrote the manuscript, obtained financial support, and provided final approval of the manuscript. Z.-Q.Y. conceived and designed the study, obtained financial support, and provided final approval of the manuscript.

CONFLICTS OF INTERESTS

The authors declare no competing interests.

ACKNOWLEDGMENTS

We thank Prof. Yue Huang's lab at the Chinese Academy of Medical Sciences, School of Basic Medicine Peking Union Medical College, Beijing, China, for the valuable training and insightful advice on ESC maintenance and differentiation. This work was supported by the National Natural Science Foundation of China (81770972), the Military Key Program (BWS13C015), the National Basic Research Program of China (2013CB967002), and the Chongqing Science and Technology Commission of China (cstc2018jcyjAX0386).

Received: May 1, 2017
Revised: May 31, 2021
Accepted: June 1, 2021
Published: July 1, 2021

REFERENCES

Akrouh, A., and Kerschensteiner, D. (2013). Intersecting circuits generate precisely patterned retinal waves. Neuron *79*, 322–334.

Bian, B., Zhao, C., He, X., Gong, Y., Ren, C., Ge, L., Zeng, Y., Li, Q., Chen, M., Weng, C., et al. (2020). Exosomes derived from neural progenitor cells preserve photoreceptors during retinal degeneration by inactivating microglia. J Extracell Vesicles *9*, 1748931.

Borghuis, B.G., Tian, L., Xu, Y., Nikonov, S.S., Vardi, N., Zemelman, B.V., and Looger, L.L. (2011). Imaging light responses of targeted neuron populations in the rodent retina. J. Neurosci. *31*, 2855–2867.

Ceto, S., Sekiguchi, K.J., Takashima, Y., Nimmerjahn, A., and Tuszynski, M.H. (2020). Neural stem cell grafts form extensive synaptic networks that integrate with host circuits after spinal cord injury. Cell Stem Cell *27*, 430–440 e435.

Chen, X., Chen, Z., Li, Z., Zhao, C., Zeng, Y., Zou, T., Fu, C., Liu, X., Xu, H., and Yin, Z.Q. (2016). Grafted C-Kit^{+}/SSEA1^{-} eye-wall progenitor cells delay retinal degeneration in mice by regulating neural plasticity and forming new graft-to-host synapses. Stem Cell Res. Ther. *7*, 191.

D'Cruz, P.M., Yasumura, D., Weir, J., Matthes, M.T., Abderrahim, H., LaVail, M.M., and Vollrath, D. (2000). Mutation of the receptor tyrosine kinase gene mertk in the retinal dystrophic RCS rat. Hum. Mol. Genet. *9*, 645–651.

Decembrini, S., Martin, C., Sennlaub, F., Chemtob, S., Biel, M., Samardzija, M., Moulin, A., Behar-Cohen, F., and Arsenijevic, Y. (2017). Cone genesis tracing by the Chrnb4-EGFP mouse line: evidences of cellular material fusion after cone precursor transplantation. Mol. Ther. *25*, 634–653.

Eiraku, M., Takata, N., Ishibashi, H., Kawada, M., Sakakura, E., Okuda, S., Sekiguchi, K., Adachi, T., and Sasai, Y. (2011). Self-organizing optic-cup morphogenesis in three-dimensional culture. Nature *472*, 51–56.

Gonzalez-Cordero, A., West, E.L., Pearson, R.A., Duran, Y., Carvalho, L.S., Chu, C.J., Naeem, A., Blackford, S.J., Georgiadis, A., Lakowski, J., et al. (2013). Photoreceptor precursors derived from three-dimensional embryonic stem cell cultures integrate and mature within adult degenerate retina. Nat. Biotechnol. *31*, 741–747.

Katz, L.C., and Shatz, C.J. (1996). Synaptic activity and the construction of cortical circuits. Science *274*, 1133–1138.

Koffler, J., Zhu, W., Qu, X., Platoshyn, O., Dulin, J.N., Brock, J., Graham, L., Lu, P., Sakamoto, J., Marsala, M., et al. (2019). Biomimetic 3D-printed scaffolds for spinal cord injury repair. Nat. Med. *25*, 263–269.

Koso, H., Satoh, S., and Watanabe, S. (2007). C-Kit marks late retinal progenitor cells and regulates their differentiation in developing mouse retina. Dev. Biol. *301*, 141–154.

Lakowski, J., Han, Y.T., Pearson, R.A., Gonzalez-Cordero, A., West, E.L., Gualdoni, S., Barber, A.C., Hubank, M., Ali, R.R., and Sowden, J.C. (2011). Effective transplantation of photoreceptor precursor cells selected via cell surface antigen expression. Stem Cells *29*, 1391–1404.

Lakowski, J., Gonzalez-Cordero, A., West, E.L., Han, Y.T., Welby, E., Naeem, A., Blackford, S.J., Bainbridge, J.W., Pearson, R.A., Ali, R.R., and Sowden, J.C. (2015). Transplantation of photoreceptor precursors isolated via a cell surface biomarker panel from embryonic stem cell-derived self-forming retina. Stem Cells *33*, 2469–2482.

Lamba, D.A., Gust, J., and Reh, T.A. (2009). Transplantation of human embryonic stem cell-derived photoreceptors restores some visual function in CRX-deficient mice. Cell Stem Cell *4*, 73–79.

Liu, Y., Chen, S.J., Li, S.Y., Qu, L.H., Meng, X.H., Wang, Y., Xu, H.W., Liang, Z.Q., and Yin, Z.Q. (2017). Long-term safety of human retinal progenitor cell transplantation in retinitis pigmentosa patients. Stem Cell Res. Ther. *8*, 209.

Luo, J., Baranov, P., Patel, S., Ouyang, H., Quach, J., Wu, F., Qiu, A., Luo, H., Hicks, C., Zeng, J., et al. (2014). Human retinal progenitor cell transplantation preserves vision. J. Biol. Chem. *289*, 6362–6371.

MacLaren, R.E., Pearson, R.A., MacNeil, A., Douglas, R.H., Salt, T.E., Akimoto, M., Swaroop, A., Sowden, J.C., and Ali, R.R. (2006). Retinal repair by transplantation of photoreceptor precursors. Nature *444*, 203–207.

Mandai, M., Fujii, M., Hashiguchi, T., Sunagawa, G.A., Ito, S., Sun, J., Kaneko, J., Sho, J., Yamada, C., and Takahashi, M. (2017). iPSC-derived retina transplants improve vision in rd1 end-stage retinal-degeneration mice. Stem Cell Reports *8*, 69–83.

Mullen, R.J., and LaVail, M.M. (1976). Inherited retinal dystrophy: primary defect in pigment epithelium determined with experimental rat chimeras. Science *192*, 799–801.

Mullen, R.J., Buck, C.R., and Smith, A.M. (1992). NeuN, a neuronal specific nuclear protein in vertebrates. Development *116*, 201–211.

Ortin-Martinez, A., Tsai, E.L., Nickerson, P.E., Bergeret, M., Lu, Y., Smiley, S., Comanita, L., and Wallace, V.A. (2017). A reinterpretation of cell transplantation: GFP transfer from donor to host photoreceptors. Stem Cells *35*, 932–939.

Pearson, R.A., Barber, A.C., Rizzi, M., Hippert, C., Xue, T., West, E.L., Duran, Y., Smith, A.J., Chuang, J.Z., Azam, S.A., et al. (2012). Restoration of vision after transplantation of photoreceptors. Nature *485*, 99–103.

Pearson, R.A., Gonzalez-Cordero, A., West, E.L., Ribeiro, J.R., Aghaizu, N., Goh, D., Sampson, R.D., Georgiadis, A., Waldron, P.V., Duran, Y., et al. (2016). Donor and host photoreceptors engage in material transfer following transplantation of post-mitotic photoreceptor precursors. Nat. Commun. *7*, 13029.

Prusky, G.T., Alam, N.M., Beekman, S., and Douglas, R.M. (2004). Rapid quantification of adult and developing mouse spatial vision using a virtual optomotor system. Invest. Ophthalmol. Vis. Sci. *45*, 4611–4616.

Sanges, D., Simonte, G., Di Vicino, U., Romo, N., Pinilla, I., Nicolas, M., and Cosma, M.P. (2016). Reprogramming Muller glia via in vivo cell fusion regenerates murine photoreceptors. J. Clin. Invest. *126*, 3104–3116.

Santos-Ferreira, T., Llonch, S., Borsch, O., Postel, K., Haas, J., and Ader, M. (2016). Retinal transplantation of photoreceptors results in donor-host cytoplasmic exchange. Nat. Commun. *7*, 13028.

Scholl, H.P., Strauss, R.W., Singh, M.S., Dalkara, D., Roska, B., Picaud, S., and Sahel, J.A. (2016). Emerging therapies for inherited retinal degeneration. Sci. Transl. Med. *8*, 368rv366.

Singh, M.S., Balmer, J., Barnard, A.R., Aslam, S.A., Moralli, D., Green, C.M., Barnea-Cramer, A., Duncan, I., and MacLaren, R.E. (2016). Transplanted photoreceptor precursors transfer proteins to host photoreceptors by a mechanism of cytoplasmic fusion. Nat. Commun. *7*, 13537.

Waldron, P.V., Di Marco, F., Kruczek, K., Ribeiro, J., Graca, A.B., Hippert, C., Aghaizu, N.D., Kalargyrou, A.A., Barber, A.C., Grimaldi, G., et al. (2018). Transplanted donor- or stem cell-derived cone photoreceptors can both integrate and undergo material transfer in an environment-dependent manner. Stem Cell Reports *10*, 406–421.

West, E.L., Pearson, R.A., MacLaren, R.E., Sowden, J.C., and Ali, R.R. (2009). Cell transplantation strategies for retinal repair. Prog. Brain Res. *175*, 3–21.

Zhou, P.Y., Peng, G.H., Xu, H., and Yin, Z.Q. (2015). C-Kit(+) cells isolated from human fetal retinas represent a new population of retinal progenitor cells. J. Cell Sci. *128*, 2169–2178.

Zou, T., Gao, L., Zeng, Y., Li, Q., Li, Y., Chen, S., Hu, X., Chen, X., Fu, C., Xu, H., et al. (2019). Organoid-derived C-Kit(+)/SSEA4(−) human retinal progenitor cells promote a protective retinal microenvironment during transplantation in rodents. Nat. Commun. *10*, 1205.

Stem Cell Reports, Volume *16*

Supplemental Information

Synaptic repair and vision restoration in advanced degenerating eyes by transplantation of retinal progenitor cells

Xiang-Yu He, Cong-Jian Zhao, Haiwei Xu, Kang Chen, Bai-Shi-Jiao Bian, Yu Gong, Chuan-Huang Weng, Yu-Xiao Zeng, Yan Fu, Yong Liu, and Zheng-Qin Yin

Supplemental Information

Figure S1

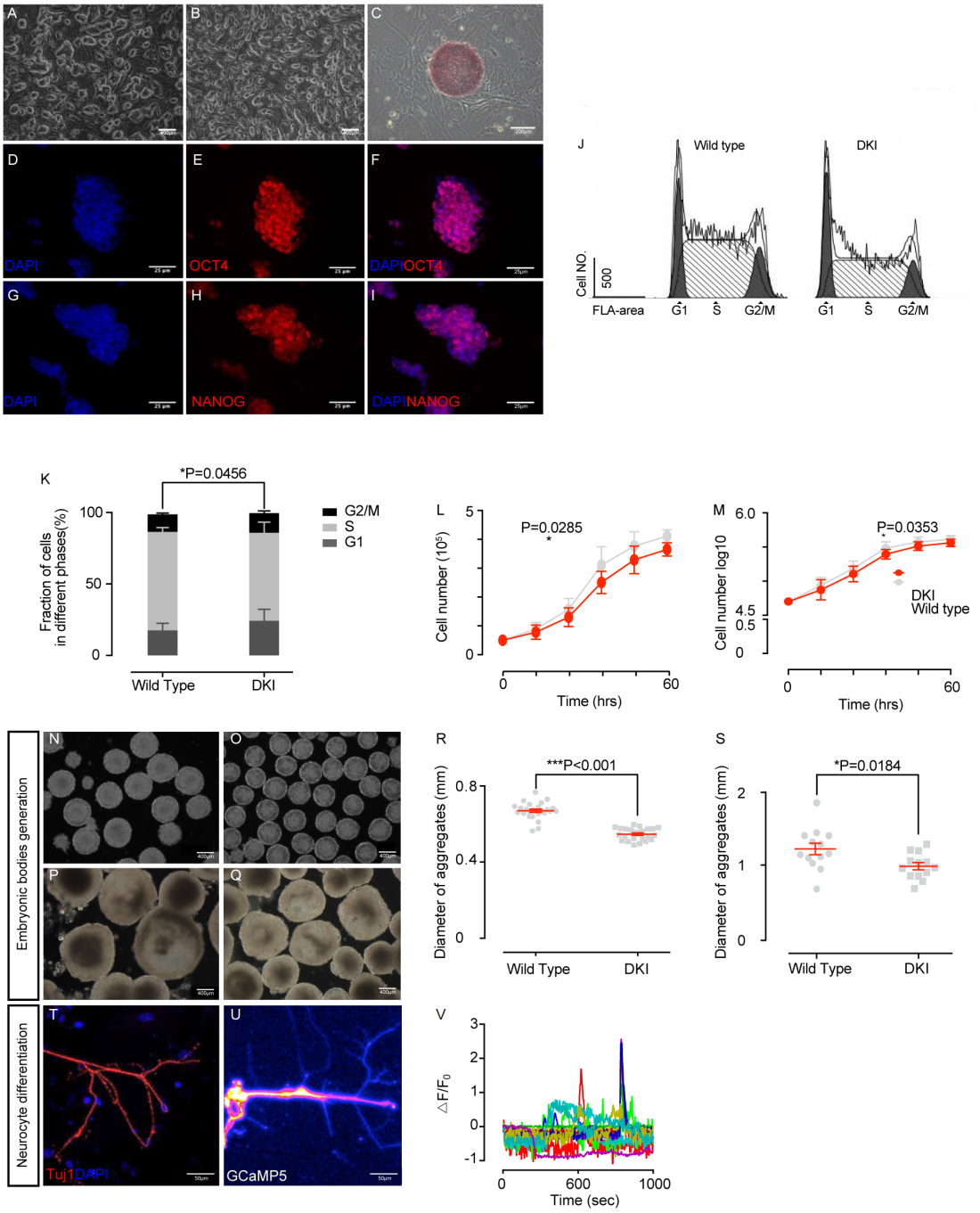

Figure S1 | *C-kit-mCherry; Rosa26-lsl-GCaMP5* mESC line characterization and capability of differentiation in *C-kit-mCherry; Rosa26-lsl-GCaMP5* mESCs, Related to Figure 1.

A, B, Image of mES cell colonies cultured in ES medium + LIF (2000 units/ml) on feeders (Mouse Embryonic Fibroblast, MEF); wild type mESCs (**A**), *C-kit-mCherry; Rosa26-lsl-GCaMP5* mESC lines (**B**). **C,** ES cell colony stained for alkaline phosphatase (red). **D-I,** Presence of pluripotency genes OCT4, NANOG in the *C-kit-mCherry;*

Rosa26-lsl-GCaMP5 mESCs colonies at passage five. **J, K,** Cell cycle assay. After 24-h serum starvation in maintenance medium containing 0.5% fetal bovine serum (FBS), cells were planted in 24 wells plate in a density of 5*10^4 with medium containing 15% FBS. Cells were then incubated for a further 24h and implemented for cell cycle assay. 81.08 ± 1.79% of wild type mESCs were in the G2 and S phases. 75.36 ± 3.89% of *C-kit-mCherry; Rosa26-lsl-GCaMP5* mESCs were in the G2 and S phases. Error bars, mean ± SEM (n = 4 independent experiments, FACS cell cycles were determined by BD Calibur and Igor Pro v. 6.10) *p <0.05, **p < 0.01 and ***p < 0.001, by paired t test. **L, M,** Growth curve of mESC at a total density of 5,000cells/cm^2, and the cell numbers were counted for further 60 hours. (n=4 of independent experiments, cell numbers were counted by Hemocytometer) *p <0.05, **p < 0.01 and ***p < 0.001, by paired t test.). **N-S,** Formation of embryoid bodies(EBs) by hanging drop method (300 cells per drop); Size comparison of EB formation of wild type mESC (Wild Type) (**N**) and EB formation of *C-kit-mCherry; Rosa26-lsl-GCaMP5* mESC (DKI) (**O**) at incubation day 2 (**R**); Size comparison of EB formation of wild type mESC (**P**) and EB formation of *C-kit-mCherry; Rosa26-lsl-GCaMP5* mESC (**Q**) at incubation day 4 (**S**). Error bars, mean ± SEM (n = 3 independent experiments with 75 aggregates counted per experiment). *p <0.05, **p < 0.01 and ***p < 0.001. **T-V,** Differentiation of *C-kit-mCherry; Rosa26-lsl-GCaMP5* mESC into neural cells; Immunofluorescence of neural specific microtubules proteins Tuj1 (T) and its autonomous calcium spikes by recording GCaMP5 fluorescence response (U, V). Scale bar: 400μm(A-C, N-Q), 50 μm (T, U) and 25μm(D-I).

Figure S2

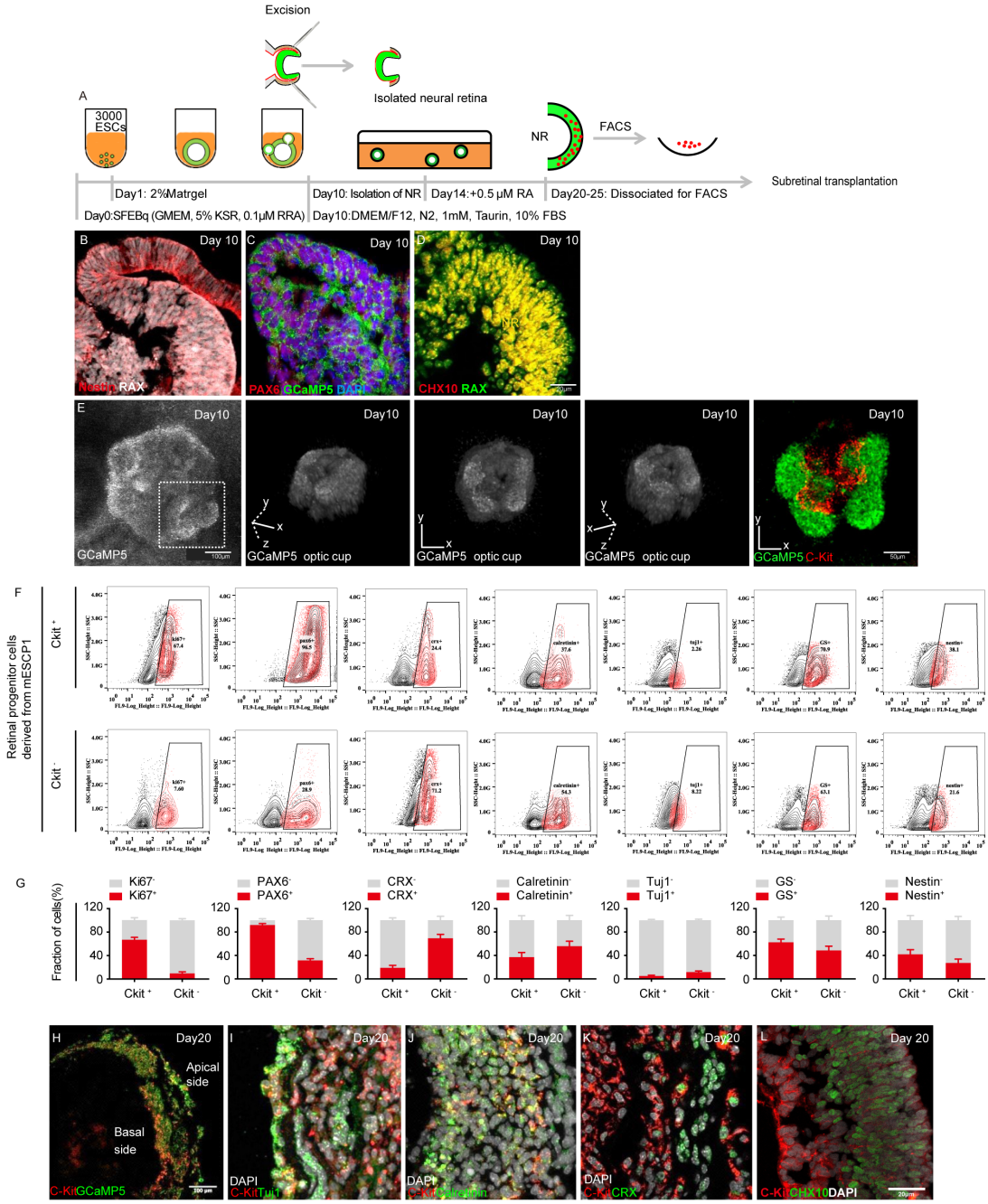

Figure S2| Three dimensional optic cup culture and FACS analysis of mEROs-derived C-kit^{+} retinal progenitor cell (RPC) co-express with retinal progenitor cell (RPC) markers, Related to Figure 1 and Figure 2.

A Schematic cartoon showing the process of retinal organoid differentiation in 3D culture system. Briefly, differentiation was initiated by the re-aggregation of dissociated DKI mESCs (3,000 cells) in a V-bottomed 96-well plate (Sumitomo Bakelite) filled with modified retinal differentiation medium (RDM) containing the retinoic acid receptor antagonist (RRA) AGN193109, and the knockout serum replacement (KSR) content was increased to 5% to

reflect a synergistic effect with Matrigel (BD Biosciences) to promote retinal anlage formation (Decembrini et al., 2014). Under these conditions, the mESC-derived continuous neuroepithelium generated four to eight optic vesicles that had evaginated from the main body; these vesicles gradually invaginated to form two-wall cup-like structures on day 10 of culture (Figure 1B-E, Figure S3E). Then, we mechanically isolated optic cups from the main aggregates at day 10. The 500 nM all-trans RA (Sigma-Aldrich) was supplemented between day 14 and 16 only. Normoxic conditions were used throughout the culture period.**B-D** Both of the inner portion (neural retina) and outer wall (pigment epithelium) expressed neural identify markers Nestin and PAX6 (**B, C**). Within optic cup-like structure, the neural retina strongly expressed retinal progenitor markers RAX and CHX10 (**B, D**) on differentiation day 10. **E** Surface-rendering of 3D-reconstructed images of GCaMP5 labelled optic cups. The right panel shows the C-kit-mCherry signal (red) was focused on the basal side of the NR. **F, G** To investing mEROs-derived C-kit^{+}/SSEA1^{-} co-express with retinal progenitor cell (RPC) markers, we examined the expression of various RPC markers PAX6 (for ganglion and amacrine cells), CRX (for photoreceptor cells), Calretinin (for amacrine cells), Tuj1 (for early stage of ganglion cells and amacrine cells), GS (for glia), Nestin (immature or glia cells) and that of the cell proliferation marker Ki67 in P1 C-kit^{+}/SSEA1^{-} cells. Among the RPC markers, Ki67, PAX6, GS and Nestin expression were detected in 66.800±4.225%, 91.833±2.685%, 62.467±5.575% and 41.711±8.088% of the cells in the C-kit^{+} cell population, respectively. CRX, Calretinin, and Tuj1 expression maintained in C-kit^{+}/SSEA1^{-} cells but was lower than in C-kit^{-}/SSEA1^{-} cells. **H-L** Immunofluorescence of 3D NR. C-kit signals were observed at the basal side of central NR (**H**) and were colocalized with retinal cell markers including Tuj1, Calretinin, CRX and CHX10 (**I-L**) post differentiation. Scale bar: 100μm (E left panel, H), 50 μm (E right panel) and 20μm (B-D, I-L).

Figure S3

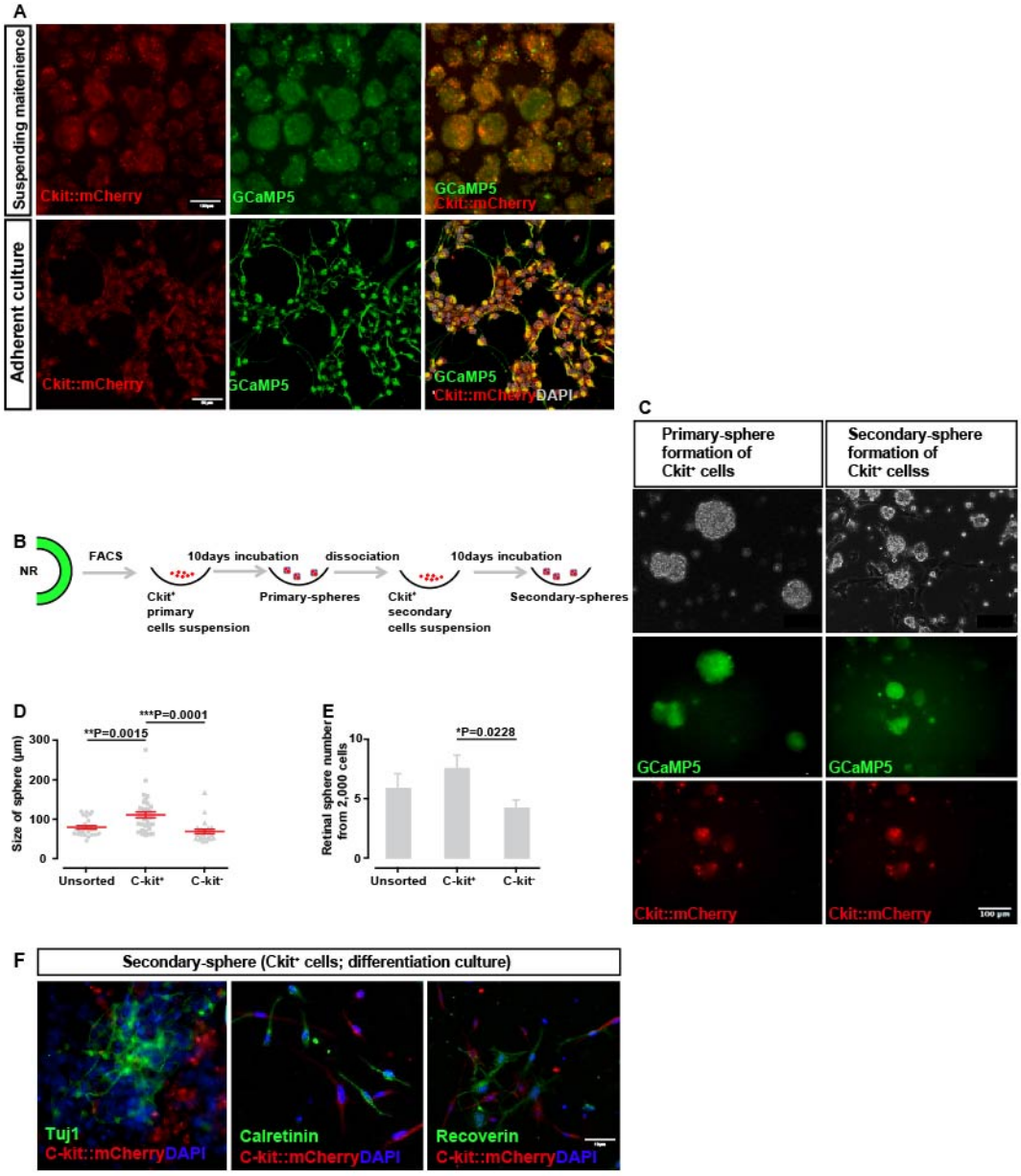

Figure S3 | Proliferation and differentiation of mEROs-derived C-kit^{+} retinal progenitor cell (RPC), Related to Figure 2.

A,B mEROs-derived C-kit^{+}/SSEA1^{-} cells were able to form colonies both in suspension and adherence conditions like fetal progenitors. **C** we confirmed the contribution of C-kit to colony-sphere formation. The cells were then subjected to culture with progenitor culture medium (1,000 cells per well). For comparison, we used unsorted SSEA1^{-} cells and C-kit^{-}/SSEA1^{-} cells from the same NR. The primary colony spheres were observed after 7-14 days of incubation. Cells that were subsequently dissociated from these colonies also showed

the same ability to form secondary spheres (1,000 cells per well). **D** The number of spheres formed by C-kit^{+}/SSEA1^{-} cells was significantly higher than the number spheres formed by C-kit^{-}/SSEA1^{-} cells. **E** C-kit^{+}/SSEA1^{-} cells formed larger spheres than C-kit^{-}/SSEA1^{-} cells. Although C-kit^{-} cells retained the capacity for sphere formation, C-kit^{+} cells play a major role in cell proliferation and colony-sphere formation at this stage of retinal differentiation and further verify the self-renewal capability of C-Kit^{+} cells. **F** To examine the differentiation ability of these cells, we applied a retinal specific differentiation protocol to P1 C-kit^{+}/SSEA1^{-} cells. After 2 weeks of incubation, the cells derived from spheres expressed fate-specific retinal cell markers, such as Tuj1 (ganglion and amacrine cells), Calretinin (amacrine cells), Recoverin (photoreceptors). This result indicates that mEROs-derived C-kit^{+}/SSEA1^{-} cells had the potency to differentiate into a subset of retinal neurons and gliacytes.

Figure S4

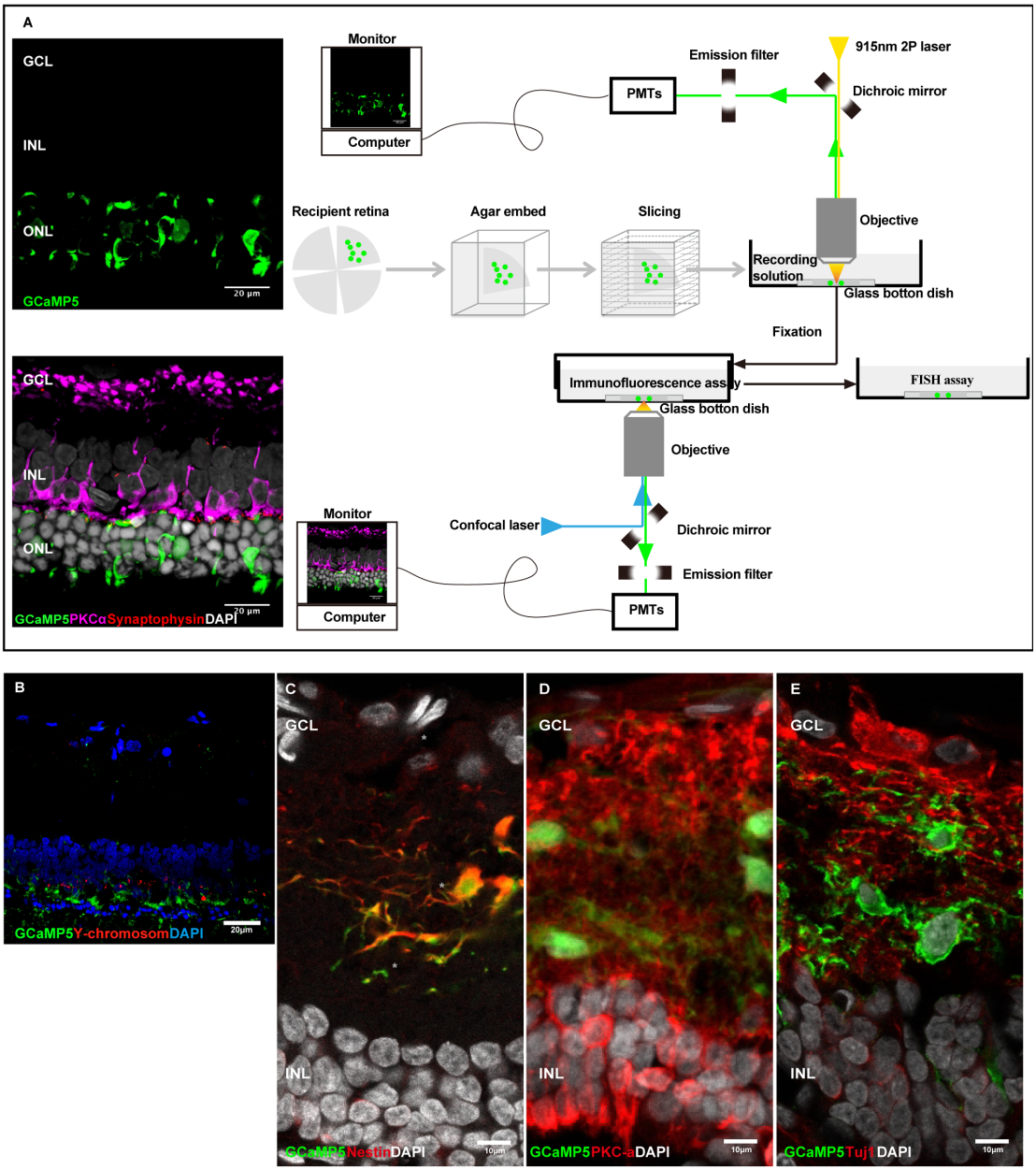

Figure S4 | Schematic of Two-photon laser-scanning on live retinal slices combined with immunofluorescence assay and confocal microscope imaging and immunofluorescence experiments on the migrated donor cells in the IPL layer, Related to Figure 3 and Figure 4.

A The upper panel presented preparation of low-gelling temperature agar-embedded live retina slice. During Two-photon laser scanning, light entering the “green” PMT was filtered with dichroic mirrors (Chroma Technology), with bandpasses set to collect GCaMP fluorescence. Then in site fixation of retinal slice was performed before immunofluorescence and FISH

assay. The lower panel presented that retinal slice was examined by confocal microscope scanning. **B** Examples of retinal sections co-stained for both GCaMP5 and Y chromosome following transplantation. **C-E** Representative images of the GCaMP5^{+} donors in the IPL layer Co-stained with markers nestin (precursor cells) (C), PKCα (bipolar cells) (D) and Tuj1 (ganglion cells) (E). Scale bar: 20μm (A, B) and 10 μm (C-E).

Figure S5

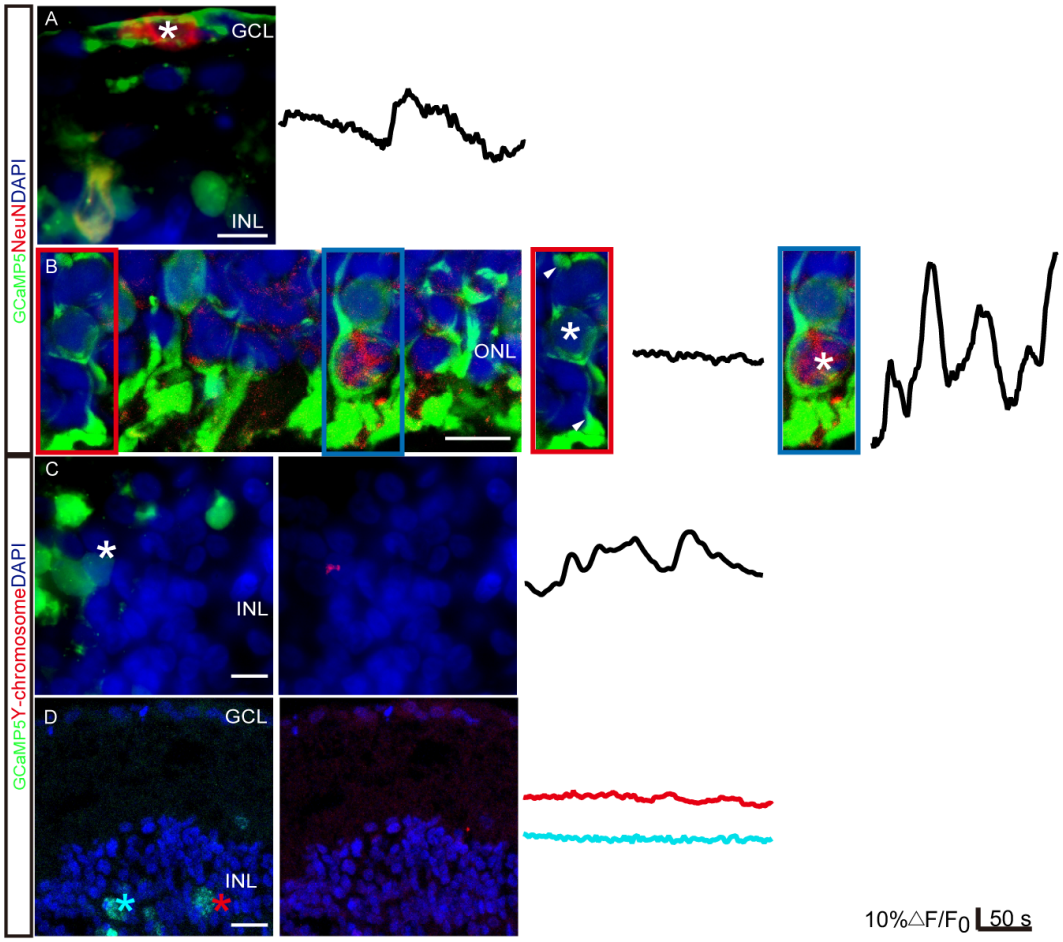

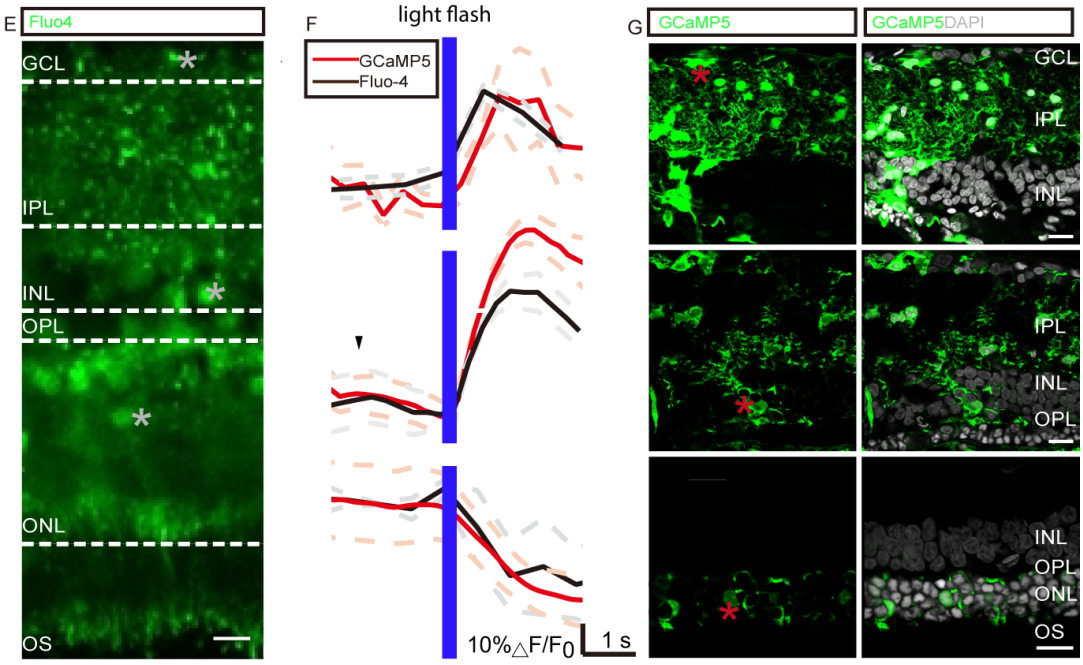

Figure S5 | Differences in morphologies and calcium signals arising from implanted cells versus those arising from material transfer and similar light stimulus-evoked

fluorescence changes were detected in both the donor cells implanted to the three retina layers (GCL, INL, ONL) and the retina neurons of the intact corresponding layers, Related to Figure 4 and Figure 5.

A, B The implanted GCaMP^{+} cells labeled with NeuN (NeuN^{+}) showed GCaMP fluorescence activity, while a proportion of cells that were not labeled with NeuN (NeuN^{-}) showed GCaMP fluorescence quiescence. **C, D** Quantification of Y^{+} nuclei in the same slice after two-photon laser scanning, data had shown that NeuN- cells with GCaMP fluorescence-active were immature in morphology and positive for Y-probe staining (n=116/116, N=4), whereas NeuN^{-} cells without GCaMP fluorescence were negative for Y-probe staining (n=372/372, N=4). **E** To test whether the implanted cells work like normal retina neurons, we compared Ca2^{+} activities of implanted cells with those of normal congenic rats. Live retinal slice of normal congenic rats (rdy^{+} rats) were labeled with calcium indicator Fluo-4 AM (green fluorescence). **F** Fluorescence response to a brief blue light flash (458 nm LED, 125 ms duration, 100 μW/cm2); The traces show fluorescence responses representative for the labeled neuron types shown in **E, G** (red and black solid lines; average ± SEM shown in dashed lines). The arrowhead indicates fluorescence response evoked by scan laser onset. **G** Fluorescence images of GCaMP-expressing donors implanting at the three retina layers (GCL, INL and ONL). Two-photon microscopy resolved all labeled structures. Images represent the average fluorescence image obtained from 3 to 10 no-flash trials. Scale bar: 10μm (A-C, E) and 20μm (D, G).

Supplemental Experimental Procedures

Animals

RCS rats and congenic control RCS-*rdy*$^{+}$ rats were maintained in the animal facilities maintained by the Institutional Animal Care and Use Committee of the Third Military Medical University. In the retinal degeneration recipient group, the adult rats were 21 days old at the time of cell injection. All treatments were conducted in accordance with NIH guidelines for the care of laboratory animals and the ARVO Statement for the Use of Animals in Ophthalmic and Vision Research. The animals were housed under a standard 12-hr light-dark cycle. All visual function tests were conducted within the light phase. All recipients were restricted to drinking water containing 210 mg/l cyclosporine A starting from the day before transplantation to the day of euthanization.

mESC maintenance

The maintenance medium for ESC contained 500 ml of Glasgow minimum essential medium (GMEM, Gibco), 5.1 ml of 100× NEAA (Gibco), 5.1 ml of 100× pyruvate (Gibco), 0.91 ml of 55 mM β-mercaptoethanol, 58 ml of KSR (Gibco) and 58 ml of FBS (fetal bovine serum, Ausbian, serum batches should be screened for plating efficiency, colony morphology, and toxicity to mESC maintenance). A final concentration of 2,000 U ml^{-1} LIF (leukaemia inhibitory factor, Millipore) was freshly added to the maintenance medium prior to culture medium change.

mESCs were placed in 60 mm tissue culture plates (Thermo Fisher) containing radially inactivated mouse embryonic fibroblasts (MEFs). When the cell colonies had grown to 80% confluence, the cells were dissociated (Gibco, 0.05% trypsin) and resuspended. The cell suspension (5-10×10^{6} cells) was then added to a plate with a fresh 60 mm feeder (MEF) layer, containing 5 ml of maintenance medium.

Flow cytometry cell cycle assay

After 24-h serum starvation in maintenance medium containing 0.5% fetal bovine serum (FBS), cells were planted in 24 wells plate in a density of 5*10^4 with medium containing 15% FBS. Continue to incubate cells for a further 24h, the cells were fixed after cooling in 70% ethanol solution for 12 hours and were then stained using the Cycletest^{TM} Plus DNA Reagent Kit (BD Bioscience). DNA content was determined using a FACSCalibur Flow Cytometer, and the data were analyzed using the ModFit 2.0 software.

mEROs differentiation culture

For retinal differentiation, mESCs were treated with modified serum-free floating cultures of embryoid-body-like aggregates with quick re-aggregation (SFEBq)(Eiraku et al., 2011). Briefly, from differentiation day 0 to day 7, dissociated C-kit mCherry Rosa 26 GCaMP5 mESCs (3,000 cells) were reaggregated in V-bottomed 96-well plates (Sumitomo Bakelite). The retinoic acid receptor antagonist (RRA) AGN193109 (0.1 μM, Toronto Research Chemicals) and Matrigel (2% [vol/vol], Corning 354230, growth factor reduced, *LDEV-free) were added to RDM (retinal differentiation medium) containing 500 ml of GMEM (Gibco), 25 ml of KSR (Gibco), 5.1 ml of 100× NEAA (Gibco), 5.1 ml of 100× pyruvate (Gibco), and 0.91 ml of 55 mM β-mercaptoethanol. From day 8 to day 9, optic neural retinas were pinched off the RPE-like portion (Watchman's forceps; FST Biology no. 5, Dumont) and transferred to retinal maturation medium containing Dulbecco's modified Eagle's medium (DMEM)/F-12 medium (Gibco), with 1% N2 (Gibco), 10% FBS, 0.5 mM all-trans retinoic acid (Sigma), 1 mM L-taurine (Sigma), 0.25 mg ml^{-1} Fungizone (Gibco), 100 U ml^{-1} penicillin and 100 mg ml^{-1} streptomycin (Gibco).

Dissociation of 3D neural retinas and FACS analysis

Neural retinas (day 8-35, from 96 aggregates per sample, n=3) containing C-kit: mCherry^{+} cells were gently dissociated into single cells via digestion with papain (papain-based kit, Sumitomo Bakelite) at 37°C for 30 min. For fluorescence-activated cell sorting (Beckman), dissociated single cells were incubated with fluorochrome-conjugated anti-SSEA1 antibody (5 μl for 1×10^{6} cells; BD Pharmingen^{TM} 562277). The details of the procedures were performed as previously described[12], and the cells were sorted by gating of GCaMP^{+}/C-kit: mCherry^{+} and SSEA1^{-}.

Sphere formation and differentiation of C-kit^{+} RPCs

After cell sorting, each type of cell (unsorted, C-kit^{+}, C-kit^{-}) was seeded into low-adherence 96-well plates at a density of 2,000 cells per well and cultured under 5% CO_2, 37°C for 10 days in sphere-formation medium containing DMEM/F12-Glutamax medium, 2% B27 (without vitamin A, Gibco), 5% FBS, 1% N2 (Gibco), 20 ng ml^{-1} human bFGF (PeproTech), 20 ng ml^{-1} human EGF (PeproTech), 5 μg ml^{-1} heparin (Sigma), 0.25 mg ml^{-1} Fungizone (Gibco), 100 U ml^{-1} penicillin and 100 mg ml^{-1} streptomycin (Gibco).

For 3D NR-derived C-kit mCherry^{+} RPC differentiation, dissociated cells were plated in PDL (poly-D-lysine) and laminin-coated dishes and further feed with RPC differentiation medium which contained DMEM/F12-Glutamax medium, 1% N2 supplement (Gibco), 10% FBS, 0.5 mM all-trans retinoic acid (Sigma), 1 mM L-taurine (sigma), 0.25 mg ml^{-1} Fungizone (Gibco),

100 U ml^{-1} penicillin and 100 mg ml^{-1} streptomycin (Gibco).

Retinal progenitor cell transplantation

C-kit^+ RPCs were prepared from C-kit mCherry Rosa 26 GCaMP5 mESC-derived nonpigmented 3D NR at differentiation day 20. Cells were manually dissociated using a papain-based kit (Worthington Biochemical). FACS-sorted C-kit^+ RPCs were collected and resuspended at a final concentration of 200,000 cells/µl in sterile ice-cold PBS (on ice) containing DNase (0.005%) prior to transplantation.

Surgery was performed under ophthalmoscopy (Leica). Recipient 63-day-old RCS rats were anaesthetized via intraperitoneal injection of pentobarbital sodium (1.5% [wt/vol], 0.2 ml/100 g). A Hamilton syringe with a 29-gauge needle (Hamilton, Reno, NV, USA) was tangentially inserted into the subretinal space through sclera puncture. Subsequently, 1 µl of pre-loaded cell suspension was gently injected into the subretinal space.

Optokinetic head-tracking tests

The visual acuities of both eyes were determined by quantitative measurements of the optomotor responses (head tracking) to rotating sinusoidal grating under scotopic conditions (<0.003 cds/m^2). The optomotor responses (head tracking) were driven by clockwise (left eye) - and counter-clockwise (right eye)-rotated gratings. The technician who performed the behavior tests were blinded. Each rat was placed in the center of four LCD monitors and was video recorded using an overhead camera. Once the rats were accustomed to the test environment, the trials were initiated by performing clockwise or counter-clockwise rotating sinusoidal grating with staircase-like eight spatial frequencies (0.05, 0.075, 0.1, 0.2, 0.3, 0.4, 0.5, and 0.6 cycles/degree). As the frequency increases across experiments, the test becomes more difficult, as determined using MATLAB software.

Immunofluorescence and confocal microscopy imaging

For 3D differentiation experiments, aggregates were fixed with ice-cold 4% paraformaldehyde in PBS for 30 min. For transplantation experiments, animals were sacrificed using the same protocol described for retinal slice preparation. The eyes were quickly enucleated and hemisected in ice-cold 4% paraformaldehyde (PFA) in PBS and fixed for 60 min in PFA at 4°C. All the samples were cryoprotected with 30% (wt/vol) sucrose in PBS, embedded in O.C.T. (SAKURA Tissue-Tek O.C.T. Compound 4583) and cut into 10 µm-thick cryosections at -20°C. The retinal cryosections were then dried for 10 min at 37°C and washed with 0.1 M phosphate

buffer (pH 7.4) for 5 min 3 times. The sections were subsequently preblocked for non-specific sites using PBS solution containing 10% normal goat serum, 1% bovine serum albumin and 0.5% Triton X-100 for 1 h at room temperature before incubation with the primary antibodies (C-kit (1:500; Cell Signalling. 3074); SSEA1 (mouse, 1:200, Santa Cruz. SC21702); Nanog (rabbit, 1:500; Millipore. AB5731); Oct4 (rabbit, 1:500; Abcam, ab19857); Rx (rabbit, 1:500; Abcam, ab86210); MiTF (mouse, 1:1000; Abcam. Ab80651); PAX6 (rabbit, 1:500; BioLegend. 901301); Vsx2 (mouse, 1:200; Boster. BA1589); Nestin (mouse, 1:500; Millipore. MAB353); CRX (rabbit, 1: 500; Novus. NBP1-88059); Recoverin (rabbit, 1:2000; Chemicon. AB5585); Pkc-α (mouse, 1:500; Santa Cruz. sc8393); Calretinin (rabbit, 1:2000; Swant. 7697); Tuj1 (mouse, 1:500; Beyotime, AT809); CRALBP (mouse, 1:500; Abcam, Ab15051); Opsin (mouse, 1:2000; Sigma, O4886); Synaptophysin (rabbit, 1:500; Cell Signalling, 5461); Ctbp2 (goat, 1:500; Santa Cruz, sc5966); and Ki67 (rabbit, 1:400; Cell Signalling, 9129)) overnight (12 h) at 4°C. After rewarming for 1 h at room temperature, the sections were rinsed 5×5 min with PBS, prior to incubation with an appropriate fluorescently labeled secondary antibody (1:1000; Invitrogen) for 1 h at room temperature. After rising 5×5 min with PBS, the sections were stained with DAPI (Abcam, Ab104139). The primary antibody was omitted in the negative controls. All sections were observed using a confocal microscope (Zeiss LSM 880).

Supplemental Reference

Decembrini, S., Koch, U., Radtke, F., Moulin, A., and Arsenijevic, Y. (2014). Derivation of traceable and transplantable photoreceptors from mouse embryonic stem cells. Stem Cell Reports 2, 853-865.

Eiraku, M., Takata, N., Ishibashi, H., Kawada, M., Sakakura, E., Okuda, S., Sekiguchi, K., Adachi, T., and Sasai, Y. (2011). Self-organizing optic-cup morphogenesis in three-dimensional culture. Nature 472, 51-56.